nature

REVIEWS

Nature Reviews revision guidelines for authors

Review articles

Nature Reviews publishes timely, authoritative articles that are of broad interest and exceptional quality. Thank you for taking the time to help us to ensure that our articles meet these high standards.

Review articles in *Nature Reviews* journals provide accessible, authoritative and balanced overviews of a field or topic. These articles are targeted towards readers from advanced undergraduate level and upwards, including researchers, academics and clinicians, and should be accessible to readers working in any discipline.

Please note that all *Nature Reviews* articles will be thoroughly edited before publication and all figures will be redrawn by our in-house art editors. Therefore, on resubmission, please send me the individual figure files via email so I can send them on to our in-house art team. All figures must be provided in high resolution (min 300dpi), editable format (PDF, EPS or AI). This is so that the art editors can modify them to conform with style. If figures are produced one program and modified in another before being coverted to EPS/PDF, the 'placed' images are not editable. PNG or PJEG are also not editable.

I have placed specific comments throughout the text, please also consider the following points when revising your manuscript:

- All figures are cited in order (Figure 1 must be cited before figure 2. If Figure consists of multiple panels, then if called out only individually, 1a, 1b, 1c and so on must be cited before figure 2 also.)
- The main sentence clause should focus on the key findings/implications of figures/articles, not the figures/articles themselves. That is, sentence structure should be as 'Nature Reviews Earth & environment publishes across three key themes (Figure 1)', and not 'Figure 1 shows the three key themes of Nature Reviews Earth & Environment'.
- Figure captions need to begin with a short (<1 line) boldface 'title' describing the essence of the figure. Captions themselves need to ensure all components of the figure are adequately defined (lines, symbols and so on). If figures are adapted from other publications, that must be specified at the end of the caption.
- Figures should not use the jet/rainbow colour bar, and red and green should be avoided together to increase clarity for colour-blind readers.
- Title should be a maximum of 87 characters, including spaces. Punctuation should be avoided.
- First and second level headings need to be 32 characters or less including spaces. Some text must be included between a first and second level header (for example, a couple of sentences explaining a general intro to the section)
- Numbered or itemised lists are not permitted. Text must be written as full prose.
- Please provide author contribution and competing interests at the end of the main text.
- Acknowledgements are optional.

- Please don't forget to refresh the references using your reference manager after the revisions; please ensure that references *are cited sequentially in the following order: main text, tables, figure legends and then boxes*. The numbered references should be listed at the end of the article. For more details on reference format please consult the Guidelines to Authors.

No single model for super-sized eruptions and their magma bodies

Colin J.N. Wilson[1*], George F. Cooper[2], Katy J. Chamberlain[3], Simon J. Barker[1], Madison L. Myers[4], Finnigan Illsley-Kemp[1] and Jamie Farrell[5]

*corresponding author email: colin.wilson@vuw.ac.nz

[1]School of Geography, Environment and Earth Sciences, Victoria University of Wellington, PO Box 600, Wellington 6140, New Zealand

[2]School of Earth and Environmental Sciences, Cardiff University, Cardiff CF10 3AT, UK

[3]Environmental Sustainability Research Centre, University of Derby, Derby DE22 1GB, UK

[4]Department of Earth Sciences, Montana State University, Bozeman, MT 59717, USA

[5]Department of Geology and Geophysics, University of Utah, Salt Lake City, UT 84112, USA

ORCID identities:
Barker: 0000-0002-3090-1403
Chamberlain: 0000-0002-2010-6182
Cooper: 0000-0002-8818-3328
Farrell: 0000-0003-0620-6168
Illsley-Kemp: 0000-0002-7114-033X
Myers: 0000-0003-2271-4445
Wilson: 0000-0001-7565-0743

Abstract

The largest explosive volcanic eruptions on Earth ('supereruptions') generate widespread ash-fall blankets and voluminous ignimbrites with accompanying caldera collapse. However, the mechanisms of generation, storage and evacuation of the parental silicic magma bodies remain controversial. In this Review, we synthesise field and laboratory evidence from Quaternary supereruptions to illustrate the great diversity in these phenomena. Despite their size, some supereruptions started mildly over weeks to months before escalating into climactic activity, whereas others went into vigorous activity immediately. Some eruptions occupied days or weeks, and others were prolonged over decades. Some were sourced from single bodies of magma, and others from multiple magma bodies that were simultaneously or sequentially tapped. In all cases the crystal-richer, deeper roots (>10 km) of the magmatic systems had lifetimes of tens to hundreds of thousands of years or more. In contrast, the erupted magmas were assembled at shallower depths (4-10 km) on shorter timescales, sometimes only centuries. Geological knowledge of past events, combined with modern geophysical techniques, demonstrates how large silicic caldera volcanoes (with past supereruptions) operate today. Future research is needed particularly on the processes behind modern volcanic unrest and the signals that might herald an impending eruption, regardless of size, at such volcanoes.

Introduction

Large explosive volcanic eruptions, labelled a supereruption **[G]** at their most extreme (>10^{15} kg or >~450 km^3 of magma, equivalent to >~1000 km^3 of pumice and ash[1]), represent an end-member of volcanic hazards specifically and of natural hazards in general[2-4]. Reaching volumes that can be 1-2 orders of magnitude greater than any explosive eruption in historic times and inevitably associated with large-scale caldera **[G]** collapse, such events are rare globally (roughly one per 100,000 years[1-3]), but offer unique insights into the diversity of large-scale magmatic processes that occur in the

Earth's crust[5-7]. The causes and triggers of such eruptions and behaviour of their parental magmatic systems are often explained through generalised models. However, consideration of available evidence suggests that there is great diversity in almost all aspects of these phenomena.

All supereruptions considered here (*n* = 13: Figure 1) have occurred at volcanoes that are positioned on continental crust. Most are associated with subduction systems or major tectonic boundaries, apart from Yellowstone, which is associated with an intraplate hot spot (Table 1). The magmas discharged in such eruptions are broadly silicic and cover a range in compositions from (generally) crystal-richer dacites (65-71 wt % SiO_2) to (generally) crystal-poorer rhyolites (71-78 wt % SiO_2). Although typically erupted from storage bodies at shallow depths (<5-10 km), it has long been recognised that these magma compositions reflect magmatic systems **[G]** that span the whole 15-60 km depths of the local crust[6-9].

All large silicic systems (not just those of super-size) have complex roots that are ultimately fed by mantle derived basaltic magmas[6-9], and minor amounts of the deeper, less evolved magmas also reach the surface in some eruptions, for example, in the form of mafic enclaves or late-stage pyroclastic deposits[10-14]. It is apparent that unusually high fluxes of basaltic magma are the fundamental control in fuelling the super-sized magmatic systems[7,15,16]. However, the controls on whether small to large volumes of silicic magma erupt or stay at depth to build plutons are still debated[5,17]. In addition, there is a growing consensus that for most of their histories, large magmatic systems reside dominantly in a largely crystalline state termed mush **[G]**. In this widely adopted framework[10,18-20], separation of melt-dominant **[G]** material into shallow bodies is considered a necessary precursor to rhyolitic eruptions (of whatever size), whereas if the mush itself is mobilised wholesale by thermal inputs it can also contribute in large volumes to crystal-rich dacitic or rhyolitic material (for example, Cerro Galan, Ongatiti: Table 1).

Large explosive eruptions are never isolated events in the history of a volcanic/magmatic system. Although a supereruption serves to define the arbitrary (yet widely used) term 'supervolcano'[4], there are usually (but not always: Toba, for example[21]) records of numerous smaller events prior to and following the super-sized event[22-26]. These smaller events yield snapshots of the evolving magma system and help to constrain what process led to the supereruption. Models for the growth and rupture of magma chambers, especially to super-sizes[27-31] are currently hampered by an inability to explain why a magmatic system should release small amounts of magma during its growth towards giant size, or to provide unique explanations for the mechanisms, timings and extreme volumes of the supereruptions.

In this Review, we highlight the diversity of behaviour of currently established Quaternary (last 2.6 Myr) magmatic systems that led to supereruptions and outline the spectrum of processes and timescales involved in the largest scales of silicic magma generation and eruption. We focus on case studies that are extensively documented, but also compare some aspects of these supereruptions with other examples of large Quaternary explosive eruptions worldwide. Our purposes are twofold. First, to emphasise the value of field focussed studies combined with petrological data in illuminating the nature of past supereruptions and their magmatic sources. Second, to highlight the importance of linking geological studies of past events with present-day geophysical investigations as a guide to the behaviour of modern actual (or potential) supereruptive centres **[G]**.

The eruptive record

The record preserved in eruption products is invariably the most important source of information about past supereruptions. In particular, central to understanding the development and evacuation of the parental large silicic magmatic systems are studies of the resulting deposits and juvenile material **[G]** collected in the field, such as pumice, ash and crystals (Figure 2a-c).

Nature of the eruption products.

The eruptive record for supereruptions is entirely represented by pyroclastic deposits, with only minor amounts of effusive activity before or afterwards to generate lava flows[32]. Even the largest lava flows associated with large silicic magmatic systems (for example, at Yellowstone[22]) only reach volumes of tens of cubic kilometres, a fraction of what pyroclastic products of the largest eruptions achieve (1000-10,000 cubic kilometres[1]). In turn, two closely linked kinds of pyroclastic deposits are important in the Quaternary supereruption record: widespread but thin fall deposits **[G]** that may occur on a continental or global scale (Figure 1) and ignimbrite **[G]** laid down from pyroclastic flows to tens to hundreds of metres thickness up to 100-150 km from source[32]. In addition, evacuation of the vast amounts of magma from the subsurface chamber leads inevitably to caldera collapse and substantial volumes of eruptive material are inferred to accumulate in the resulting depression as infill.

The nature and preservation of eruption products strongly influences the sampling of deposits and thus the information that can be gained about the magmatic source. Pieces of lava or individual pumices in pyroclastic deposits represent parcels of juvenile magma, so that compositional diversity or uniformity in the crystals and groundmass reflect those within the parent magma body. In contrast, compositional variations within bulk samples of pyroclastic rocks may reflect mechanical enrichment or depletion in crystals[33], or incorporation of lithic material[34] **[G]** during eruption (Figure 2a,b) and not reflect the magmatic source. If the groundmass material is glassy, it can be considered to represent quenched melt. Often, however,the groundmass will have crystallised during slow cooling (devitrified) and no longer reflect the original melt composition. Ignimbrites commonly contain large enough fragments of juvenile material (pumice: Figure 2a) so that the full nature of the magma parcel can be determined, but many ignimbrites were emplaced hot enough to compact back to solid rock under loading (weld) and devitrify such that the pumices are flattened to lenses (fiamme: Figure 2c) that are challenging to sample intact. In contrast, fall deposits (especially the large distal blankets deposited coevally with the ignimbrites[35-37]) are rapidly quenched against the surrounding air, meaning that they preserve largely unaltered glass compositions[38-41]. These deposits are dominated by ash-sized shards and loose crystals which, when coupled with their layer-by-layer deposition, can yield an unambiguous chronology of any compositional diversity or zonation within the original magmatic system[6,7,42].

Timing of eruptions.

For individual eruptions, a commonly held view based on historical examples is that the larger the event, the higher the eruption rate and hence that super-sized events may not last much longer than small events[3,43]. Some refer to even the largest events as occupying hours to days[22], yet there is often a lack of field evidence to constrain such conclusions. Studies of size grading in deep-sea ashes were used to suggest durations of days to weeks for the Youngest Toba, Indonesia and Los Chocoyos, Guatemala[44,45] eruptions. Any direct links established between fall deposition (that can be modelled through plume dynamics[46-48]) and coeval ignimbrite generation, however, allow the timing of ignimbrites to be constrained. In the case of the Bishop, the incoming of the Glass Mountain rhyolite lithics[34] is used to link fall deposits and ignimbrite (Figure 2d,e) and demonstrate that they were coevally emplaced[49]. Using estimates of fall deposit deposition times, the Bishop eruption can then be inferred to have occupied roughly 1 week[10,49]. Longer durations for the Bishop eruption were inferred from welding variations in the ignimbrite[50], but such variations may have no chronological significance[51] (Figure 2e).

The large-scale emplacement of ignimbrite and the onset of caldera collapse are widely inferred to be coeval[34]. As such, examples such as Youngest Toba[21,36], Whakamaru[52], Ongatiti[53] and Cerro Galan deposits[54], all of which lack initial fall deposits, are inferred to have begun abruptly, with collapse of the chamber roof occurring early on. Others commenced with fall deposits vented from single or multiple vents. The transition into caldera collapse may then have occurred gradationally (Oruanui) or likely rapidly (Bishop, Tshirege, Otowi, Huckleberry Ridge) as the chamber roof began to collapse along ring fractures[34,49,55-57].

There is also a range of timings within individual eruptions. Some, like the Bishop, Youngest Toba and Cerro Galan show no evidence in their deposits for substantial time breaks whereas others show evidence for spasmodic activity. For instance, the first fall unit of the Oruanui eruption was deposited, then enough time elapsed (some months[55]) for the distinctive white ash to be reworked by burrowing animals before fall unit 2 was emplaced (Figure 2f). Subsequent activity also included three pauses long enough for the eruption plume to dissipate and minor erosion to occur[48]. Early activity of the Huckleberry Ridge eruption occupied some weeks on the basis of wind reworking of the initial fall deposits (Figure 2g)[58]. This activity was followed by three ignimbrite members (A-C) being emplaced without hiatuses internally, but with their mutual contacts showing evidence of time breaks (Figure 2h). In particular, along the Teton River gorge near Newdale, Idaho, member A was emplaced over a weak substrate that deformed under the load, distorting the welding fabric in the ignimbrite into domical folds cored by the remobilised underlying sediments. There was enough timing for this process to occur and the top surface of member A to partially cool, such that member B was chilled against it and is not deformed, suggesting a break of weeks to months. Members A and B together then had largely cooled in this area before member C was emplaced and was chilled against the underlying material to deposit vitric (glassy) material, suggesting a break of years to a few decades[12]. In most of the examples we consider here, however, this information has not yet been determined, or is very challenging to interpret from the limited exposures available (for example, at Toba).

Bracketing eruptive events.

Preceding and subsequent eruptions supply information on the state of the magmatic system before and after the main event, although the former case is sometimes hampered by the evidence (particularly of lava domes) being destroyed during caldera collapse. Thousands to ten thousand years prior to the climactic event, the Huckleberry Ridge system had a precursor lava dome[22]. There were multiple events before the Oruanui, Lava Creek and Otiwi eruptions[22,25,59,60] but others of the eruptions we consider had no preserved precursors. We are able to more thoroughly evaluate the larger dataset of the eruptions following the main event, representing the recovery time of these large systems. For instance, the first eruptions after the Youngest Toba event were effusive, occurring 5-15 kyr later[61], post-Oruanui explosive activity came about 5 kyr later[23] and Bishop effusive activity came no more than ~17 kyr later[24]. In contrast, there are substantially longer gaps (100-200 kyr) in the eruptive record at Yellowstone between the Huckleberry Ridge and Lava Creek eruptions and their respective oldest-known younger (effusive) events[22]. The magmas erupted after the shorter time breaks generally show evidence for magmatic rejuvenation, sometimes in the form of hotter, crystal-poor rhyolite (for example, after the Bishop[24]) or as dacitic material that compositionally resembles the feedstock magma for subsequent rhyolite generation (for example, after the Oruanui[23]). In an extreme case, however, the Mangakino magmatic system in New Zealand evacuated a compositionally similar large (200 km^3) ignimbrite (Rocky Hill) only decades after the Kidnappers supereruption[62]. Magmas erupted after longer time breaks (as at Yellowstone[22,63,64]) are of comparable composition to the main events and it appears that the longer dormancy period allows for a fuller recovery of the magmatic system to rhyolitic eruptive compositions. In all cases, however, the whole crustal-scale magmatic system undergoes change after the supereruptive event, with evidence for renewed influxes of deeper seated, less evolved magmas and assimilation of existing mush and country rocks around the magma reservoir[23,24,65].

Cyclic activity of caldera systems.

Within the eruptive sources of the Quaternary examples of supereruptions considered here, there is a wide spectrum of longer-term behaviour. At one extreme, the Bishop[26], Cerro Galan[54] and Los Chocoyos[37] supereruptions represent by far the largest events at their respective volcanic centres and there were no other eruptions there of a size large enough to induce caldera collapse. In contrast, the Valles[56,66], Yellowstone[22] and Toba[21] centres have each seen two supereruptions, plus at least one additional eruption large enough to generate caldera collapse in the last two cases. The

Aso-4 eruption represents the youngest and largest of four caldera-forming events focussed within a limited area at that centre[14]. The four New Zealand examples (Table 1; Figure 1) collectively are encompassed within a geographic area of similar size to the Yellowstone system but represent discrete multi-cycle foci of magma generation and eruption[67]. All four supereruptive events were followed by additional caldera-forming eruptions, Kidnappers after only one to two decades[62], Whakamaru by about 10 kyr[68], Oruanui by about 23.5 kyr[23], and the Ongatiti by about 30 kyr[67].

The controls on these complex relationships have not been fully explored although models have been proposed to relate eruptive compositions and the growth of magmatic systems to sizes capable of caldera-forming (although not super-) eruptions[69,70]. However, there are demonstrable temporal variations in such key parameters as mafic magma supply rates into the system roots[16,26] and external tectonic controls in building and releasing large volumes of magma[11,58,71,72] that render generalised modelling problematic. In two of the New Zealand cases, the younger, smaller caldera-forming events discharged almost identical magmas (Kidnappers[53], Whakamaru[52]), whereas in the Oruanui example, the younger eruptions involve a magmatic system that generated contrasting compositions[23].

The nature of supereruptive magmatic systems

Views on the nature of large silicic magmatic systems have changed over the last few decades from that of a unitary long-lived melt-dominated magma body to complex configurations of pre-eruptive magmatic generation and storage (Figure 3). These new views arise from five lines of evidence considered in the following sub-sections.

Long-term generation and storage domains.

Silicic magmas are now widely inferred to be generated and stored over the long term (tens to hundreds of thousands of years) in vertically extensive crystal-rich mush zones, rather than within large melt-dominant bodies, which are now though to be short lived features (centuries to thousands of years). Earlier models had the issue of how to separate crystals from melt to drive the fractionation processes[7,73]. The now widely adopted mush model reversed the process to separate the melt from the crystals, which is dynamically much easier [18-20,26]. Enhancements of this model (which is not universally accepted, however[74]) consider the processes of reactivation and/or melt extraction from the mush and the relevant timescales involved[75-78].

The area of caldera collapse can provide an estimate of the areal extent of the evacuated portion of the magmatic system[79], but this can be misleading if there is peripheral slumping and/or lateral drainage of magma[55,80-82]. If the caldera area is divided into the erupted volume, the average vertical extent of the melt-dominant body or bodies can be estimated and typically is of the order 1-3 km[6]. These bodies can then be positioned in the crust using storage pressure estimates from melt inclusions or mineral geobarometry[83] or thermodynamic calculations of phase equilibria[84,85].

Mostly beneath (but also around) the bodies tapped during the eruption there is the mush zone of intruded materials trending towards less evolved compositions (ultimately to the mantle-derived basaltic melts[16]). This deeper zone has long been recognised[6,7] but is now commonly referred to as a 'trans-crustal magmatic system'[9]. The architecture of this column can only be inferred for Quaternary systems[23,86,87], but from older examples where the crustal cross-section has been exposed these systems are compositionally zoned overall with complex internal geometries[88-90]. Deeper parts of the systems, where intermediate composition magmas (andesites) are generated, are inferred from surface erupted compositions[26,91,92] and considered from numerical modelling[8,93]. A large proportion of magmatic differentiation occurs within these lower crustal regions, prior to the establishment of pre-eruptive melt dominant magma bodies. However, the petrological record from these regions is limited by the fact that the majority of the crystal cargo will remain in lower crustal mushy material or is diluted by later crystals formed in the mid- to upper-crust from the much larger volumes of more differentiated melt.

Through the identification of distinct crystal textures and populations in erupted products, it is possible in some cases to identify the relative extent of crystal growth within both the crystal-rich mush and the melt-dominated regions of the magmatic system (Figure 4). Such studies show that the extent of interaction between any melt-dominant reservoirs and their source mush varies greatly. This interaction has been inferred to take the form of one of the following. First, wholesale eruption of the remobilised mush itself (plus any separated melt-dominant bodies), producing crystal-rich rhyolitic (for example, Ongatiti[53]) or less evolved deposits (for example, Cerro Galan[94]). At one extreme (not seen in Quaternary supereruptions) this mush remobilisation generates the very crystal-rich dacitic ignimbrites labelled as 'monotonous intermediates'[7]. It is often inferred that mobilisation of melt and crystals from the mush requires 'defrosting' by an input of heat and or volatiles[19,75-78]. Second, remobilisation and rapid extraction of melts (plus entrained crystals) from an underlying source mush[18,78,95-100]. At an extreme, in the Oruanui, the melt-dominant body is inferred to have been generated in <600 years and mostly in <200 years[11] prior to the eruption. In addition, ~90% of the plagioclase and orthopyroxene cores in the Oruanui high-silica rhyolite pumices are inherited from sources that span the entire compositional ranges of those crystals erupted in the whole 2 Myr history of the Taupō Volcanic Zone[11]. Third, transport of melt but very few crystals from the mush into the melt-dominant magma body. Only a small fraction of crystals in the Bishop Tuff, for example, can be linked back to the underlying mush: most appear to have grown in the melts in which they were erupted[10,101] and accumulation of the melt-dominant body is inferred to have been prolonged and piecemeal[10].

The thermal (hence physical) state of these mush systems remains a subject of controversy. Based on an apparent disparity between the long-term records for mush systems and the short-term records indicated from diffusion studies in crystals it has been proposed[102,103] that the mush is in a state ("cold storage") close to or below the solidus (<~700 °C) for most of its history. In this state, diffusive processes are effectively arrested and melts and crystals are remobilised and extracted only shortly before eruption[102,103]. However, this model requires unusual thermal circumstances. For example, once the volatiles are lost from the system as it approaches the solidus the reheating process has to reach the relevant dry solidus temperature in order to remobilise the crystal mush. This temperature is much higher than the magmatic temperatures of the erupted products and would profoundly affect the record in the crystals. The disparities in timescales from the crystal records used to propose cold storage remain an issue that requires explanation. Alternatively "warm storage" has also been proposed[104], where the long-term state of the mush entails that up to a few tens of percent melt be present. This is enough melt to maintain some crystal growth, but overall the mush is too crystal-rich (>50-60 volume percent[105]) to readily erupt without an additional process such as melt separation or remobilisation coming into play. Geophysical evidence beneath several modern silicic systems (for example, at Toba[87]; Yellowstone[86]; Laguna del Maule, Chile[106]) show the presence of modest amounts of melt (5-15 volume %), more consistent with the warm storage concept.

Conditions of magma storage.

There are three aspects of the shallow magmatic system and the generation and storage of eruptible silicic melt-dominant bodies that are considered here. The first aspect concerns the number of pre-eruptive magma bodies. In contrast to the long held view of single bodies feeding the entire eruption (driven by the Bishop Tuff example[7,10]), improved geochemical data coupled with more detailed field studies and sampling, have frequently indicated the presence of compositional clustering, particularly for the largest examples considered here. This feature points towards the simultaneous and/or sequential tapping of multiple separate melt-dominant magma bodies[12,41,42,58,107]. There is thus a spectrum of behaviour (Figure 3).The systems feeding the Bishop, Ongatiti and Aso-4 eruptions appear to have been single bodies[10,14,53,94]. That for the Oruanui was also a single large body but was invaded by a foreign, unrelated, silicic magma during the early stages of its eruption[11,72]. In contrast, those for the Kidnappers[42,95], Whakamaru[52], Youngest Toba[41,107] and Huckleberry Ridge[12,57,58] deposits were erupted from multiple separate bodies. In the Huckleberry Ridge case, not only were the melt-dominant bodies separate, but also their root zones, whereby the whole eruption represents the evacuation of at least four separate magmatic systems[12,57,58]. As the configuration of magma bodies at depth strongly interacts with (and is influenced by) the crustal stress field, with implications for long-term magma chamber stability and eruption triggering mechanism(s), discerning how many discrete magma bodies contribute to an eruption has important implications[27].

The second aspect concerns the nature and presence of compositional zonation within the magma body, whether due to variations in the abundance of crystals (increasing downwards) or the composition of the melt phase (becoming less evolved downwards), or both (for example, Bishop[10,101]). Although once considered to be ubiquitous[6,7], compositional variations in these large eruptions are not always present (Table 1), and can arise from a number of possible causes. Some systems show diversity in compositions, but these need not be systematically displayed in the eruptive ordering (for example, Oruanui[11]; Huckleberry Ridge[12]; Youngest Toba[107]). Other examples preserve a degree of orderly compositional stratification in the deposits that is linked to zonation in the magma body (Bishop[10]; Aso-4[14]). The melting of earlier cumulate **[G]** crystals (separated out from the melt in which they grew) and/or remobilisation of mush material has been proposed as a means to account for geochemical and isotopic zonations preserved in large silicic deposits[78,108] and is seen in the extreme trace element variations in the Huckleberry Ridge system[12]. However, in other cases, the compositionally distinct melts contributing to the zonation appear to be less-evolved precursors to the dominant more evolved magma[10,101]. Notably, those systems that record a signature of rapid melt extraction from the mush system (for example, Oruanui[11], Kidnappers[62,95]) lack evidence for compositional stratification within the melt-dominant magma bodies and appear to have been vigorously convecting when tapped by eruption.

The third aspect concerns the depths and conditions for pre-eruptive magma storage. Although certain characteristics appear to be consistent between these voluminous eruptions, including the relatively narrow apparent range of pre-eruptive temperature (700-950 °C) and minimum storage depths (4-8 km: Table 1), these parameters represent transitory states of the magma reservoir and could be limited by the methods used to evaluate them (Figure 4). Although crystal specific studies provide records of the evolutionary history, these records are themselves limited to recording conditions where the relevant phase is stable. For example, our understanding of pressures, and thus depths, of storage often is determined by volatile (H_2O and CO_2) solubility relationships from quartz-hosted melt inclusions (for example, Bishop[109,110]). Quartz, however, will only stabilise late in the crystallisation sequence, meaning that it lacks an older history and thus will only preserve the conditions associated with late stage storage (Figure 4)[111,112]. Such limitations can be overcome through use of a broader range of mineral indicators[11,113], however this requires those minerals to be present in the crystallising magma body. In addition, in the Oruanui, 90% of the plagioclase and orthopyroxene crystals in single pumices have cores that were inherited from older rocks[11]. Use of crystal abundances in eruption products to model the evolution of magmas towards a predicted state where eruption is triggered[114] is thus invalidated if the crystals are inherited. Some systems are more suited to a full reconstruction of intensive parameters because of the availability of large pumice clasts that have experienced limited post-depositional alteration and were rapidly quenched upon eruption (for example, Bishop, Oruanui). For those systems where these criteria are not met (for example, Lava Creek[22]), our current understanding of magma storage conditions is severely more limited.

Integrating these petrological models for the number, zonation, temperature and depth of magmatic storage regions highlights that the magma reservoirs feeding large silicic eruptions are architecturally diverse[79,115,116]. Yet, there is a tendency to classify storage regions into either being more ‘tank-like’ or “‘dispersed’[117]. For instance, based on the modelled pressure ranges of the storage volume versus the caldera collapse area, the Oruanui, Bishop and Toba systems are considered ‘tank-like’, whereas the Huckleberry Ridge system is considered more ‘dispersed’[117]. However, variably available data limit the application of this approach, (particularly in the case of the Huckleberry Ridge[12]) and, to a first order, the configuration tells us little about what came next. For example, two ‘tank like’ systems[117], Bishop and Oruanui, show overlapping model storage pressures and temperatures, yet the Bishop ‘tank’ preserved an internal zonation (thermal and volatile[10,101,109,118]) and erupted rapidly and continuously, whereas the Oruanui ‘tank’ was remarkably well-stirred and the eruption was spasmodic[11,55,72].

A diversity of timescales.

The body or bodies of melt-dominant material that lead to eruption can accumulate over a range of timescales, from tens of thousands of years down to centuries[11,62,113,119-121]. These timescales highlight a contrast between the longer-term history of the magmatic system, during which processes of mafic influx, assimilation (of country rocks or earlier crystallised products of the system) and fractionation occur, versus the shorter timescales for physical assembly of eruptible magma bodies. Development of the overall magma system can be quantified through radiometric age-dating of preceding eruptions, which ultimately shows that the activity associated with supereruptions may date back hundreds of thousands of years[26,92], but can be as short as a few tens of thousands of years[59]. Assessment of the magmatic histories preserved in eruption products involves two methods that yield complementary perspectives. The first is U-Pb or U-Th techniques used to date crystallisation ages of U- and/or Th-rich accessory phases that are commonly present in the rhyolites that form the dominant volume of melts tapped in supereruptions (Box 1). The second is diffusion geochronometry, which assesses the relative timing of formation of a compositional boundary through the consequent time-dependent diffusive relaxation of this boundary within crystals. These boundaries and extracted timescales can be linked to specific processes through detailed petrological study.

Absolute age **[G]** dating of accessory phases (principally zircon, but also other U, Th-bearing accessory phases[122-124]) has shown that records of large silicic volcanic systems are relatively short (tens to hundreds of thousands of years) when compared with their older plutonic counterparts that typically record zircon crystallisation timescales spanning millions of years[5,125,126]. Among the extensive literature of zircon age data there is a diversity in the age spectra preserved within supereruption deposits. Unimodal age spectra, with minimal or no recycling of zircons from previous magmatic events, are seen in the Bishop[121], Ongatiti[127] and Huckleberry Ridge[100,128] deposits. These spectra reflect mush systems with zircon formed early in the geochemical evolution of these bodies, and then continuing to crystallise. In contrast, zircon age spectra from the Oruanui[59, 129], Kidnappers[127], Cerro Galan[130] and Youngest Toba[131] deposits all have multiple peaks, indicating episodic growth or recycling of earlier magmatic systems. The lack of recycled zircons within systems like the Bishop and Huckleberry Ridge suggests that rather than super-sizing a pre-existing magmatic system[6,132], any earlier magmatic systems are effectively reset. This would imply that the supereruptive events required a strong change in storage conditions, such as thermal resetting of the system[26]. On the basis of the zircon and other age data, it is apparent that large silicic magmatic systems do not accumulate and crystallise on any special timescale, and that the amount of magma eventually erupted is not simply related to the time over which the mush system or its melt-dominant bodies have been extant.

In contrast to absolute age dating, relative age **[G]** timescales inferred from diffusion studies are more focussed on shorter-lived processes, such as the extraction of melt from the mush and its accumulation into eruptible, melt-dominated bodies[11,62,113], or the disturbance, for example, by mafic mixing into a crystallising silicic magma body, eventually leading to eruption[98,99,133]. These timescales are commonly based on modelling the relaxation of an originally sharp compositional boundary within mineral phases using diffusion chronometric techniques[134]. Such boundaries are inferred to be generated by the changes in growth conditions accompanying the disturbance of the mush or transport of the crystal between the mush and melt-dominant body. Diffusion-based timescales require an original step boundary to be approximated within the crystal, where distinguishing between profiles generated by diffusive relaxation versus mineral growth can be problematic[134]. In some large silicic systems the timescales of destabilisation and/or accumulation appear to be on the order of decades to centuries prior to eruption, despite the large size of the magma bodies[11,99]. Such short timescales appear to apply also to smaller-scale caldera-forming eruptions of silicic magmas[62,96,135], implying that a common suite of processes may be involved. Other large examples, like the Bishop and Youngest Toba show evidence for more gradual changes approaching the climactic outburst[131,133].

Structural controls on location and eruption dynamics.
The locations of large silicic systems in the Quaternary can be linked in general to tectonic setting[136]. In addition, although a range of models are available that propose why and when these large eruptions occur when they do, many of these models treat the melt-dominant body as a system isolated from the external stress field, then propose singular causes for eruption triggering[27-31,137]. However, there is increasing evidence for the role of external tectonic forces in controlling both the location of magmatic systems and the dynamics of magma accumulation and release[30,58,72]. For the former, note that most of the systems summarised in Table 1, although often in convergent margin settings, are in areas of extension and/or (particularly in the case of Toba[138]) strike-slip tectonics. The Bishop deposits were vented from the largest of a series of magmatic systems, active over several million years, erupting from a transtensional region at the juncture of the Sierra Nevada microplate and the extensional Basin and Range province[26,71]. For the four Quaternary supereruptions in New Zealand, the interplay between volcanism, magmatism and the rift architecture has strongly influenced the position of large-scale caldera collapses[139], with caldera-tectonic linkages inferred in large eruptions[82]. Similar considerations also apply to some smaller but active silicic systems, such as Santorini, Greece[140] and Laguna del Maule, Chile[141].

There are also several lines of evidence for syneruptive tectonic controls on the nature of large eruptions. The simultaneous and sequential eruption of discrete magma bodies during the opening stages of the Huckleberry Ridge eruption is inferred to reflect vents becoming active through tectonic linkages[58]. In the case of the Oruanui event, concurrent rifting is inferred to have modulated the early stages of the eruption, as well as permitting the lateral 'invasion' of a foreign silicic magma from an adjacent, unrelated system into the super-sized Oruanui body[72]. Caldera formation is in itself an extreme example of a tectonic event, and the shapes of the calderas associated with large eruptions often reflect the orientation of tectonic elements in the shallow crust. For example, the shape and NW-SE elongation of the Oruanui structural caldera are coincident with a cross-arc soft-linkage, whereas the Whakamaru caldera margin to the north (Figure 1) is influenced by a behind-arc rift[139,142].

Geophysical studies of modern large silicic systems.
Geophysical imaging techniques (Figure 5) can provide a snapshot in time of the location, size, and state of contemporary large silicic magmatic systems and ongoing processes within them. Combining multiple geophysical techniques with geochemical/petrological data from past eruptions to constrain interpretations yields our best picture of the present-day state of large (super-sized) magmatic systems, both quiescent and restless. At present, although there is no system identified with large amounts (tens to hundreds of cubic kilometres of melt-dominant material), the resolution of imagery cannot preclude modest-sized bodies (up to the 1-10 km^3 range) from being present at Yellowstone, for example[86]. Although there is focussed attention on large silicic caldera-related systems[143,144] an important point is that unrest events do not imminently indicate an eruption and that eruptions come in all sizes, even at supereruptive centres[22,26,145]. An ultimate goal is to use modern geophysical methods along with geological knowledge of past events to provide

operationally useful forecasts around future unrest and eruptive activity; however, this goal often remains out of reach.

Due to its location and restless nature[143], Yellowstone is the most extensively geophysically studied supereruptive centre. A large amount of effort at Yellowstone has been focused on seismically imaging the magma reservoir, through controlled source experiments[146], earthquake tomography[86,147-149], and ambient noise tomography[150,151]. When combined, these studies indicate that the Yellowstone volcanic system is underlain by a large silicic upper-crustal magma reservoir organised into stacked sills and an underlying basaltic lower-crustal magma reservoir (Figure 5). These reservoirs are crystal-rich with the upper-crustal silicic reservoir containing 5-15% melt and the lower-crustal basaltic reservoir 1-2% melt[86,149]. Similar studies at Aso[152], Toba[87,138] and Taupō[153] also show evidence, through seismic, gravity and magnetotelluric surveys, that regions of partial melt presently reside beneath or close to these caldera systems. Long Valley is controversial: contrasting geophysical and geological evidence is put forward to propose or refute the presence of magma beneath the caldera[154-157]. Many large silicic systems share common attributes with Yellowstone: vigorous hydrothermal systems in the near-surface that are fuelled by more evolved magma mush systems in the mid-crust that are in turn underlain by a mafic feeder zone. These observations agree with the trans-crustal scale architecture suggested by geochemical/petrological studies[7,11,12,19,23,92] and also observed in ancient examples[88-90]. Repeat/continuous geophysical surveys then offer the opportunity to monitor any changes in modern magmatic systems.

Although geophysical surveys demonstrate that some supereruptive systems have an active, partially molten magma reservoir, none of them show evidence for the large, shallow, melt-dominant bodies that are inferred to feed supereruptions[86,138,153,155]. However, estimating melt percentages from geophysical signals is not straightforward[158,159] and, typically, tomographic results show only an averaged view of the sub-surface structure[160]. The resolution is often limited to ~5-10 km (Figure 5), reflecting the seismic wavelengths used in such studies and the typical station spacing of seismic networks. As melt-dominant bodies are thought to be ephemeral[9,116] it is possible that they are currently absent within these magmatic systems. However, geophysical imaging currently does not have the resolution to determine whether smaller bodies, still capable of producing eruptions[23,96], are present or not. Questions then arise around when these melt-dominant bodies begin to accumulate or crystallise back to mush, what geophysical signals (if any) would show, and could we detect them with current methods?

Caldera-forming volcanoes often undergo periods of elevated seismicity, ground deformation and gas emission, known as unrest (Figure 5). While it is assumed that all eruptions from large silicic systems are preceded by some level of unrest, the vast majority of unrest periods are not followed by an eruption[161]. Monitoring systems at volcanoes worldwide commonly include seismic networks, ground deformation monitoring and surficial fluid emissions monitoring. At Yellowstone for example, the Yellowstone Volcano Observatory issued a monitoring plan[162] in 2006 that stated that the monitoring system in place should "detect earth signals that indicate changes in the magmatic system that underlies Yellowstone. These signals include earthquakes, deforming ground, and increased heat, gas, or water flow". However, such monitoring depends on the ability to distinguish between normal behaviour and some transient change in behaviour (unrest) that could be related to magmatic activity. There have been numerous unrest episodes while Yellowstone has been monitored, including large seismic swarms[163-166] and episodes of accelerated ground deformation[167-169]. Similar, but less vigorous unrest episodes have also been observed at supereruptive centres at Long Valley[170-172] and Taupō[173-175], as well as at other large silicic centres such as Campi Flegrei[176,177] and Laguna del Maule[141,144]. However, none of these episodes has yet led to a volcanic eruption. This is why it is imperative that monitoring systems at large silicic volcanoes monitor for multiple signals (that is, seismic, deformation, gas release, etc.) as a change in one signal likely does not point to an impending eruption, but simultaneous changes in all signals may point to the movement of magma into the shallow crust and the possibility of eruption.

The question then arises as to whether we can define normal behaviour at these large systems versus a signal related to an impending eruption. Since there have not been eruptions at large silicic caldera-forming systems in modern (instrumented) times, this question cannot be answered definitively and there is much room for further work. Application of new tools such as machine learning algorithms[178] in monitoring systems at large silicic systems may be able to permit timely interpretation of transient signals that reflect the start of movement of magma towards the surface on the hours-to-days timescales indicated from petrological studies[58,179]. In addition, laboratory experiments linking direct measurements of melt percentage and seismic velocity[181,182] will aid in the interpretation of tomographic results with respect to the amount of melt available in a magma reservoir. There is also a need to improve our understanding of non-eruptive unrest at caldera systems[161], as these events can cause major societal and economic impacts[173,182-184]. These impacts can be exacerbated by public perceptions of supereruptive centres as liable to catastrophically erupt (particularly Yellowstone[185]), whereas in reality such an event is extremely unlikely. Therefore, effective communication of the nature and frequency of unrest at large silicic systems is a key mitigation strategy against future unrest episodes.

Summary & Future Perspectives

Synthesis of field and petrological studies of supereruption products shows that there is great diversity in the nature of these events, making it challenging when considering the current behaviour of modern systems. Supereruptions can start, literally with a bang, with collapse of the chamber roof, or begin gradually, with hesitancy before escalating into catastrophic activity. Overall, the eruption may be rapid, uninterrupted events over a few days, or an episodic sequence prolonged over decades. Magmas that feed supereruptions may come from single or multiple final storage regions, which can be zoned, or may be convectively mixed. Magmas are assembled into their eruptible states across diverse timescales, in extreme cases involving magmatic accumulation rates exceeding 1 km^3 per year. This brief review serves to emphasise three points about the present-day states of the large silicic systems that have produced super-sized or other silicic large eruptions. First, supereruptions in the past define the supereruptive centre, but do not dictate the modern behaviour of the volcano or constrain the size of future activity. The common perception of a volcano such as Yellowstone is that any future event will be catastrophic[173], yet this is most improbable. Episodes of unrest associated with movement of magma are one to three orders of magnitude more frequent than eruptions, yet perceptions of modern supereruptive systems tend to be driven by the largest, rarest events. Future work in this area needs to meld scientific knowledge of large silicic systems with education and communication to the general public.

Second, further work remains to be done around understanding supereruptive systems. There is a marked contrast between the overall long lifetimes of large silicic systems versus intermediate timescales of eruptible magma accumulation, versus the short timescales of triggering and eruption. These contrasts suggest either a remarkable uniformity of behaviour across systems of widely varying sizes, or the presence of other factors that are currently overlooked. Evidence for the timing and nature of physical processes associated with eruptions is scant, yet is important in forecasting the nature of future activity and associated hazards. Modelling these behaviours require further development, including better understanding of the role of external factors such as tectonic forces and crustal stress states influencing magma accumulation, establishing the onset and modulation of eruptions, and resolving the role of the hydrothermal envelope in causing geophysical unrest signals. In addition, current modelling of melt extraction is still largely based on the formation of a single melt dominant reservoir, without consideration for more complex configurations indicated from recent petrological studies.

Third, unrest events at a supereruptive centres may be the norm, and thus the probability of eruption (compared with non-eruptive unrest) may be one to three orders of magnitude less than that of any detected subsurface changes. Petrological studies have, however, highlighted that large silicic systems record timescales that suggest extraction and accumulation of eruptible magma can occur over periods of only a few years. The ability of a silicic system to move into a state of eruptive capability so rapidly presents challenges in the modern instrumented era, and those factors (tipping points) that cause unrest associated with the accumulation of magma to evolve into eruption remain unquantified[186]. Limited data on silicic magma rise rates suggest that once the magma begins to ascend, the warning time for eruption onset may be only days to months, giving little time for interpretation of changing geophysical signals.

Acknowledgements

This work has been supported by the Marsden Fund grant VUW0813 (Royal Society of New Zealand to C.J.N.W.), a James Cook Fellowship (Royal Society of New Zealand) to C.J.N.W., and the ECLIPSE Programme, funded by the N.Z. Ministry of Business, Innovation and Employment. G.F.C. is supported by a NERC Standard Grant (NE/T000317/1), M.L.M. is supported by an NSF CAREER grant (EAR 2042662) and S.J.B. acknowledges Marsden Fund grant VUW1627.

Author contributions

G.F.C and K.J.C conceived the idea of the manuscript. All authors drafted the manuscript, led by C.J.N.W. All authors commented on and discussed the manuscript at all stages.

Statement of competing interests

The authors declare no competing interests.

Proposed Display Items:

Figure 1: Location maps of Quaternary supereruption locations and source caldera outlines. Sources are marked by filled red circles and satellite images of the source calderas are from Google Earth®. Caldera outlines and eruptive ages are shown for Aso-4[14,189] from Aso (Japan), the Bishop [10,34] from Long Valley (USA)[26], the Huckleberry Ridge[22] and Lava Creek[22] from Yellowstone (USA), the Otowi[66] and Tshirege[97] members of the Bandelier Tuff from Valles (USA)[56], the Los Chocoyos[37] from Atitlán (Guatemala), the Cerro Galán[54] from Cerro Galán (Argentina), the Ongatiti[53] and Kidnappers[95] from Mangakino (New Zealand), the Whakamaru[52] from Whakamaru (New Zealand), the Oruanui[55] from Taupō (New Zealand) and the Oldest Toba[21] and Youngest Toba[21] tuffs from Toba (Indonesia). Examples of selected fall deposit mapped extents are shown as grey stippled regions on the world map for the Aso-4[187], Lava Creek[35], Whakamaru[40] and Youngest Toba[36] eruptions. Copyrighted images by Google (2011), Europa Technologies (2011), Tele Atlas, and Geocenter Consulting. Use of these images is consistent with usage allowed by Google (http://www.google.com/permissions/geoguidelines.html) and do not require explicit permission for publication.

Figure 2: Field and textural relationships in supereruption deposits as guides to eruption characteristics. (a) Non-welded Bishop ignimbrite, with individual pumices (P) and lithics (L) in an ash matrix[10]. (b) Welded Ongatiti ignimbrite[53], showing two kinds of silicic pumice (P1, P2), juvenile mafic (M) and lithic clasts (L). (c) Welded Bishop ignimbrite with the pumices flattened into fiamme[51]. (d): A thin wedge of Bishop ignimbrite[49] enclosed in fall material can be demonstrated from the consistent incoming of a distinctive lithic type (Glass Mountain rhyolite lava[34]) to be equivalent to and coevally emplaced with >70 metres of densely welded ignimbrite ~15 km away (panel e).(e) The density (= welding) minimum does not occur at a horizon of any stratigraphic significance and cannot be due to a prolonged time break[50] as the coeval fall deposits were continuously emplaced[49]. (f) Early fall deposits of the Oruanui eruption showing the reworking (time break) between fall units 1 and 2[55]. (g) Early fall deposits of the Huckleberry Ridge eruption, showing ripple bedding indicating wind reworking and prolonged deposition[57,58]. (h) Field evidence for time breaks during the emplacement of ignimbrite members in the Huckleberry Ridge Tuff[12]. Height of exposure is 80 m.

Figure 3: End-member pre-eruptive magmatic storage configurations for Quaternary supereruptions. (a) Multiple melt-dominant bodies that could be sequentially or simultaneously tapped during the eruption. Each body may be compositionally distinct, have unique crystal cargos and be either homogenous or zoned. (b) Single, compositionally stratified melt-dominant body. Compositional stratification (crystal content, melt composition) of the body is reflected within the deposits. (c) Single unzoned melt-dominant body, with compositional variations arising through pre- or syn-eruptive mixing of other magmas (mostly more mafic than the main evolved storage body) or rejuvenation and melting of underlying cumulates (mush) by hot mafic magmas. All three examples can be considered as trans-crustal magmatic systems, with mafic magmas intruding the lower crust and extensive, deep mush zones[6-9]. Quaternary examples of supereruptions for each type of system and process are given where inferred from detailed petrological and geochemical studies (see Table 1 for references). These configurations represent endmember examples, and processes such as magma mixing and mush rejuvenation are not limited to the examples shown. The configuration of other examples discussed in the text (Lava Creek and Cerro Galan) are yet to be fully established.

Figure 4: The mineral toolbox for probing the origins and evolution of silicic magmatic systems. The mineral phases commonly found in silicic magmas are shown with indications of their main use in unravelling one or more of the pressure, temperature and compositional evolution of the magmas, plus the associated timescales magma accumulation and eruption. Cathodoluminescence (zircon, quartz) and back-scattered electron (all other mineral phases) images from scanning electron microscopy are shown for a selection of mineral phases. The white scale bar in all images is equal to 100 microns. White open boxes indicate examples of compositional changes where diffusion modelling can be applied across the compositional variations represented by the grey tonality. Representative spot sizes are shown in the Fe-Ti oxides panel for: Electron Probe MicroAnalysis (EPMA: blue), Secondary Ion Mass Spectrometry (SIMS: magenta), Laser-Ablation Inductively Coupled Plasma Mass Spectrometry (LA-ICP-MS: red) and Fourier Transform InfraRed spectrometry (FTIR: green).

Figure 5: Schematic diagram of geophysical imaging of supereruptive systems. The figure indicates the limitations of resolution of geophysical studies together with some of the phenomena associated with unrest at large silicic systems in general. (a) A schematic view of a magma body as imaged by geophysical methods. These have revealed that modern magma bodies have a stratified structure, with the silicic mush dominated by horizontal structures (e.g. sills, shown as horizontal black lines), while the mafic feeder zone is dominated by vertical structures (e.g. dikes, shown as vertical black lines)[87,138,149-151]. Geophysical resolution is typically on the order of 5-10 km and is not sufficient to image localised melt bodies[158-160]. The crustal thickness (depth to the Moho) can be between 15 and 60 km, depending on the local setting for each volcano (Table 1). (b) Monitoring of supereruptive and other centres relies on the detection of periods of unrest, often associated with heightened seismic activity (hypocentres shown as red filled circles), ground deformation (black arrows) and/or changes to the shallow hydrothermal system (blue spirals)[161, 163-177].

(See last page for Table 1.)

Box 1: Dating accessory phases for magmatic histories

For the purpose of following the growth and development of the magmatic systems that feed silicic eruptions, accessory phases (such as zircon or allanite) lend themselves to radiogenic absolute age dating. The methods use primarily the U- and/or Th-decay series, as these minerals preferentially include U and Th and exclude Pb during crystal growth[122-124]. Subsequent changes through reequilibration are inhibited by the exceptionally slow diffusion rates of Pb through the mineral structure and so pre-eruptive ages of crystal growth remain undisturbed[193]. Various methods can be used to then date these phases, each with advantages and limitations. There is a trade-off between the precision of an age determination and the volume of material consumed, such that ultra-high precisions can normally only be obtained as average ages from whole crystals. Thus, the method employed to date accessory phases largely depends on the process(es) of interest:

1. Cross sectional in-situ analysis of polished grains using Secondary Ion Mass Spectrometry (with an ion probe[124,194,195]) or Laser-Ablation Inductively Coupled Plasma mass Spectrometry[196,197] can be used to give analyses of core, intermediary and near-rim domains within single crystals. Combining many analyses can reveal inheritance and punctuated growth of these accessory phases. Uncertainties on individual analyses are high and these can only be reduced by compiling many tens to hundreds of analyses. Estimates of eruption age within uncertainty of $^{40}Ar/^{39}Ar$ eruption ages can be obtained in favourable cases[121].
2. Surface profiling by in-situ analysis of unpolished grain surfaces can be used to date the latest stage of mineral growth, and has also been shown to yield ages within uncertainty of $^{40}Ar/^{39}Ar$ eruption ages[191]. Individually, these age determinations are relatively imprecise due to high analytical uncertainty, although multiple age determinations can be combined. In addition, the evolutionary history of the magma bodies as reflected in crystal growth is not recovered with this method.
3. Chemical dissolution of individual zircon grains for analysis by Isotope-Dilution Thermal Ionisation Mass Spectrometry yields highly precise ages (with analytical precision similar to that of $^{40}Ar/^{39}Ar$ methods[100,128,192]); but this gives an averaged age for the entire mineral grain, and obscures any growth history or inheritance.

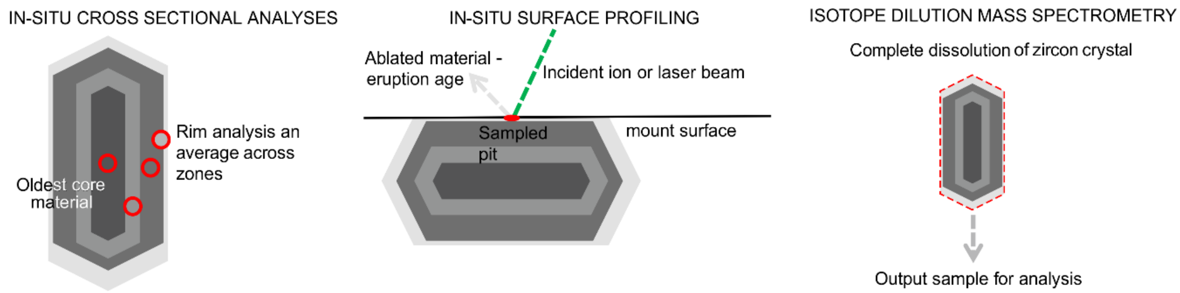

Glossary:

- **Supereruptions** – Events that discharge of more than 1 x 10^{15}kg of magma (450 km^3, or >~1000 km^3 of pumice and ash) in a single eruption
- **Caldera** – A topographic depression formed through the collapse of the Earth's surface due to the withdrawal of large volumes of magma from the upper crust
- **Magmatic system** – The entire region within the crust and upper mantle that feeds the volcanic system, including the melt dominant body or bodies and mushy, non-eruptible material
- **Mush** – A framework of crystals (>40-50 volume %) with interstitial melt, which forms a strong skeleton that can no longer easily flow or erupt due to its high viscosity
- **Melt-dominant** – material separated out from the crystal mush, consisting of 0 to 40-50% crystals, that can flow and is eruptible, but which has a short lifetime within the upper crust
- **Supereruptive centre** – A volcanic centre that has produced one (or more) supereruptions in the past, sometimes referred to as a supervolcano.
- **Juvenile material** – material that is newly discharged at the Earth's surface in an eruption
- **Fall deposits** – Deposited to millimetres to metres in thickness from high (tens of kilometres) buoyant plumes of ash, dispersed by winds over thousands to millions of square kilometres
- **Ignimbrite** – Deposits of concentrated ground-hugging pyroclastic flows, typically metres to hundreds of metres thick, covering up to thousands to tens of thousands of square kilometres
- **Lithic material** – pre-existing (country) rocks caught up as fragments in the deposits of explosive eruptions
- **Cumulate –** crystals grown in the mush that have been separated out from the melt in which they grew and hence may generate contrasting compositions of melt if re-heated
- **Absolute age** – An age determined by measurements of radioactive decay in minerals and associated with the time period since closure of the system
- **Relative age** – An age that is determined, typically through measurements of diffusion profiles in minerals, relative to the point of quenching by eruption

References

1. Mason, B. G., Pyle, D. M. & Oppenheimer, C. The size and frequency of the largest explosive eruptions on Earth. *Bull. Volcanol.* **66**, 735–748 (2004).
2. Sparks, R. S. J. *et al. Super-eruptions: global effects and future threats*. *Report of a Geological Society of London working group*. 1-24 (The Geological Society, London, UK, 2005).
3. Self, S. The effects and consequences of very large explosive volcanic eruptions. *Phil. Trans. R. Soc. Lond*. A **364**, 2073–2097 (2006).
4. Wark, D. A. & Miller, C. F. (Editors) Supervolcanoes. *Elements* **4**, 11–49 (2008).
For the non-specialist, still the single most useful collation of information about super-sized eruptions and their source volcanoes.
5. Lundstrom, C. C. & Glazner, A. F. (Editors) Enigmatic relationship between silicic volcanic and plutonic rocks. *Elements* **12**, 91–127.
6. Smith, R. L. Ash-flow magmatism. *Geol. Soc. Am. Spec. Pap.* **180**, 5–27 (1979).
7. Hildreth, W. Gradients in silicic magma chambers: implications for lithospheric magmatism. J. Geophys. Res. 86, 10153–10192 (1981).
A classic comprehensive overview and synthesis of the nature of many types of magmatic systems (including super-sized examples) that acted as a springboard for many subsequent studies.
8. Annen, C., Blundy, J. D. & Sparks, R. S. J. (2006). The genesis of intermediate and silicic magmas in deep crustal hot zones. *J. Petrol.* **47**, 505–539.
9. Cashman, K. V., Sparks, R. S. J. & Blundy, J. D. Vertically extensive and unstable magmatic systems: a unified view of igneous processes. *Science* **355**, eaag3055 (2017).
10. Hildreth, W. & Wilson, C. J. N. Compositional zoning of the Bishop Tuff. *J. Petrol.* **48**, 951–999 (2007).
11. Allan, A. S. R. *et al.* A cascade of magmatic events during the assembly and eruption of a super-sized magma body. *Contrib. Mineral. Petrol*. **172**, 49 (2017).
A comprehensive linking of physical volcanology with magmatic processes inferred from petrological data and magmatic timescales from multiple mineral phases to document the evolution of a supereruptive system.
12. Swallow, E. J., Wilson, C. J. N., Charlier, B. L. A. & Gamble, J. A. The Huckleberry Ridge Tuff, Yellowstone: evacuation of multiple magma systems in a complex episodic eruption. *J. Petrol.* **60**, 1371–1426 (2019).
13. Boro, J. R., Wolff, J. A. & Neill, O. K. Anatomy of a recharge magma: hornblende dacite pumice from the rhyolitic Tshirege Member of the Bandelier Tuff, Valles Caldera, New Mexico, USA. *Contrib. Mineral. Petrol.* **175**, 96 (2020).
14. Kaneko, K., Kamata, H., Koyaguchi, T., Yoshikawa, M. & Furukawa, K. Repeated large-scale eruptions from a single compositionally stratified magma chamber: an example from Aso volcano, Southwest Japan. *J. Volcanol. Geotherm. Res.* **167**, 160–180 (2007).
15. de Silva, S. L. & Gosnold, W. A. Episodic construction of batholiths: insights from the spatiotemporal development of an ignimbrite flare-up. *J. Volcanol. Geotherm. Res.* **167**, 320–335 (2007).
16. Barker, S. J. *et al.* What lies beneath? Reconstructing the primitive magmas fueling voluminous silicic volcanism using olivine-hosted melt inclusions. *Geology* **48**, 504–508 (2020).
17. Gelman, S. E., Deering, C. D., Bachmann, O., Huber, C. & Gutiérrez, F. J. Identifying the crystal graveyards remaining after large silicic eruptions. *Earth Planet. Sci. Lett*. **403**, 299–306 (2014).
18. Bachmann, O. & Bergantz, G. W. On the origin of crystal-poor rhyolites: extracted from batholithic crystal mushes. *J. Petrol.* **45**, 1565–1582 (2004).
This paper marked a paradigm shift in how we view magmatic systems, providing an integrated model of mush zones and the evolution of the plutonic and volcanic components of the system.

19. Bachmann, O. & Huber, C. Silicic magma reservoirs in the Earth's crust. *Am. Mineral*. **101**, 2377–2404 (2016).
20. Bachmann, O. & Bergantz, G. W. Rhyolites and their source mushes across tectonic settings. *J. Petrol.* **49**, 2277–2285 (2008).
21. Chesner, C. A. The Toba caldera complex. *Quat. Int*. **258**, 5–18 (2012).
22. Christiansen, R. L. The Quaternary and Pliocene Yellowstone Plateau Volcanic Field of Wyoming, Idaho, and Montana. *U.S. Geol. Surv. Prof. Pap.* **729-G**, 1–143 (2001).
23. Barker, S. J., Wilson, C. J. N., Allan, A. S. R. & Schipper, C. I. Fine-scale temporal recovery, reconstruction and evolution of a post-supereruption magmatic system: Taupo (New Zealand). *Contrib. Mineral. Petrol.* **170**, 5 (2015).
24. Hildreth, W., Fierstein, J. & Calvert, A. Early post-caldera rhyolite and structural resurgence at Long Valley caldera, California. *J. Volcanol. Geotherm. Res.* **335**, 1–34 (2017).
25. Troch, J. et al. Rhyolite generation prior to a Yellowstone supereruption: insights from the Island Park–Mount Jackson Rhyolite series. *J. Petrol*. **58**, 29–52 (2017).
26. Hildreth, W. Volcanological perspectives on Long Valley, Mammoth Mountain, and Mono Craters: several contiguous but discrete systems. *J. Volcanol. Geotherm. Res.* **136**, 169–198 (2004).
27. Gregg, P. M., de Silva, S. L., Grosfils, E. B. & Parmigiani, J. P. Catastrophic caldera-forming eruptions: thermomechanics and implications for eruption triggering and maximum caldera dimensions on Earth. *J. Volcanol. Geotherm. Res*. **241**–**242**, 1–12 (2012).
28. Degruyter, W. & Huber, C. A model for eruption frequency of upper crustal silicic magma chambers. *Earth Planet. Sci. Lett*. **403**, 117–130 (2014).
29. Karakas, O., Degruyter, W., Bachmann, O. & Dufek, J. (2017). Lifetime and size of shallow magma bodies controlled by crustal-scale magmatism. *Nat. Geosci*. **10**, 446–450.
30. Cabaniss, H. E., Gregg, P. M. & Grosfils, E. B. The role of tectonic stress in triggering large silicic caldera eruptions. *Geophys. Res. Lett.* **45**, 3889–3895 (2018).
31. Townsend, M. & Huber, C. A critical magma chamber size for volcanic eruptions. *Geology* **48**, 431–435 (2020).
32. Wilson, C. J. N. Supereruptions and supervolcanoes: processes and products. *Elements* **4**, 29–34 (2008).
33. Walker, G. P. L. Crystal concentration in ignimbrites. *Contrib. Mineral. Petrol.* **36**, 135–146 (1972).
34. Hildreth, W. & Mahood, G. A. Ring-fracture eruption of the Bishop Tuff. *Geol. Soc. Am. Bull.* **97**, 396–403 (1986).
Details a unique circumstance by which the use of lithic clasts within a deposit are used to reconstruct the development of an iconic caldera-forming eruption
35. Izett, G. A. & Wilcox, R. E. Map showing localities and inferred distributions of the Huckleberry Ridge, Mesa Falls, and Lava Creek ash beds (Pearlette family ash beds) of Pliocene and Pleistocene age in the western United States and southern Canada. *U.S. Geol. Surv. Misc. Inv. Ser. Map* I-1325 (1982).
36. Rose, W. I. & Chesner, C. A. Dispersal of ash in the great Toba eruption, 75 ka. *Geology* **15**, 913–917 (1987).
37. de León, A. C. *et al.* A history of violence: magma incubation, timing and tephra distribution of the Los Chocoyos supereruption (Atitlán Caldera, Guatemala). *J. Quat. Sci.* **36**, 169–179 (2021).
38. Nash, B. P., Perkins, M. E., Christensen, J. N., Lee, D. C. & Halliday, A. N. The Yellowstone hotspot in space and time: Nd and Hf isotopes in silicic magmas. *Earth Planet. Sci. Lett.* **247**, 143–156 (2006).
39. Nash, B. P. & Perkins, M.E. Neogene fallout tuffs from the Yellowstone hotspot in the Columbia Plateau region, Oregon, Washington and Idaho, USA. *PLoS ONE* **7**, e44205 (2012).

40. Matthews, N. E. *et al.* Ultra-distal tephra deposits from super-eruptions: examples from Toba, Indonesia and Taupo Volcanic Zone, New Zealand. *Quat. Int*. **258**, 54–79 (2012)
41. Pearce, N. J. G., Westgate, J. A., Gualda, G. A. R., Gatti, E. & Muhammad, R.F. Tephra glass chemistry provides storage and discharge details of five magma reservoirs which fed the 75 ka Youngest Toba Tuff eruption, northern Sumatra. *J. Quat. Sci.* **35**, 256–271 (2020).
42. Cooper, G. F., Wilson, C. J. N., Millet, M.-A., Baker, J. & Smith, E. G. C. Systematic tapping of independent magma chambers during the 1 Ma Kidnappers supereruption. *Earth Planet. Sci. Lett*. **213**–**214**, 23–33 (2012).
43. Carey, S. & Sigurdsson, H.. The intensity of plinian eruptions. *Bull. Volcanol.* **51**, 28–40 (1989).
44. Ninkovich, D., Sparks, R. S. J. & Ledbetter, M. T. The exceptional magnitude and intensity of the Toba eruption, Sumatra: an example of the use of deep-sea tephra layers as a geological tool. *Bull. Volcanol.* **41**, 286–298 (1978).
45. Ledbetter, M. T. & Sparks, R. S. J. Duration of large-magnitude explosive eruptions deduced from graded bedding in deep-sea ash layers. *Geology* **7**, 240–244 (1979).
46. Sparks, R. S. J. *et al. Volcanic Plumes*. (Wiley, Chichester, UK, 1997).
47. Baines, P. G. & Sparks, R. S. J. Dynamics of giant volcanic ash clouds from supervolcanic eruptions. *Geophys. Res. Lett*. **32**, L24808 (2005).
48. Costa, A., Suzuki, Y. J. & Koyaguchi, T. Understanding the plume dynamics of explosive super-eruptions. *Nat. Comm*. **9**, 654 (2018).
49. Wilson, C. J. N. & Hildreth, W. The Bishop Tuff: new insights from eruptive stratigraphy. *J. Geol.* **105**, 407–439 (1997).
50. Riehle, J. R., Miller, T. F. & Bailey, R. A. Cooling, degassing, and compaction of rhyolitic ash-flow tuffs: a computational model. *Bull. Volcanol.* **57**, 319–336 (1995).
51. Wilson, C. J. N. & Hildreth, W. Assembling an ignimbrite: mechanical and thermal building blocks in the Bishop Tuff, California. *J. Geol.* **111**, 653–670 (2003).
52. Brown, S. J. A., Wilson, C. J. N., Cole, J. W. & Wooden, J. The Whakamaru group ignimbrites, Taupo Volcanic Zone, New Zealand: evidence for reverse tapping of a zoned silicic magma system. *J. Volcanol. Geotherm. Res*. **84**, 1–37 (1998).
53. Cooper, G. F. & Wilson, C. J. N. Development, mobilisation and eruption of a large crystal-rich rhyolite: the Ongatiti ignimbrite, New Zealand. *Lithos* **198**–**199**, 38–57 (2014).
54. Cas, R. A. F. et al. The flow dynamics of an extremely large volume pyroclastic flow, the 2.08-Ma Cerro Galan Ignimbrite, NW Argentina, and comparison with other flow types. *Bull. Volcanol*. **73**, 1583–1609 (2011).
55. Wilson, C. J. N. The 26.5 ka Oruanui eruption, New Zealand: an introduction and overview. *J. Volcanol. Geotherm. Res.* **112**, 133–174 (2001).
56. Self, S., Goff, F., Gardner, J. N., Wright, J. V. & Kite, W. M. Explosive rhyolitic volcanism in the Jemez Mountains: vent locations, caldera development and relation to regional structure. *J. Geophys. Res.* **91**, 1779–1798 (1986).
57. Swallow, E. J. *et al.* Evacuation of multiple magma bodies and the onset of caldera collapse in a supereruption, captured in glass and mineral compositions. *Contrib. Mineral. Petrol.* **173**, 33 (2018).
58. Myers, M. L., Wallace, P. J., Wilson, C. J. N., Morter, B. K. & Swallow, E. J. Prolonged ascent and episodic venting of discrete magma batches at the onset of the Huckleberry Ridge supereruption, Yellowstone. *Earth Planet. Sci. Lett.* **451**, 285–297 (2016).
59. Wilson, C. J. N. & Charlier, B. L. A. Rapid rates of magma generation at contemporaneous magma systems, Taupo volcano, New Zealand: insights from U-Th model-age spectra in zircons. *J. Petrol.* **50**, 875–907 (2009).
60. Wilson, C. J. N., Stelten, M. E. & Lowenstern, J. B. Contrasting perspectives on the Lava Creek Tuff eruption, Yellowstone, from new U-Pb and ^{40}Ar/^{39}Ar age determinations. *Bull. Volcanol*. **80**, 53 (2018).
61. Mucek, A. E. et al. Post-supereruption recovery at Toba caldera. *Nat. Comm*. **8**, 15248 (2017).

62. Cooper, G. F., Morgan, D. J. & Wilson, C. J. N. Rapid assembly and rejuvenation of a large silicic magmatic system: insights from mineral diffusive profiles in the Kidnappers and Rocky Hill deposits, New Zealand. *Earth Planet. Sci. Lett*. **473**, 1–13 (2017).
63. Girard, G. & Stix, J. Magma recharge and crystal mush rejuvenation associated with early post-collapse Upper Basin Member rhyolites, Yellowstone caldera, Wyoming. *J. Petrol.* **50**, 2095–2125 (2009).
64. Till, C. B., Vazquez, J. A., Stelten, M. E., Shamloo, H. I. & Shaffer, J. S. Coexisting discrete bodies of rhyolite and punctuated volcanism characterize Yellowstone's post-Lava Creek Tuff caldera evolution. *Geochem., Geophys., Geosyst.* **20**, 3861–3881 (2019).
65. Troch, J., Ellis, B. S., Harris, C., Ulmer, P. & Bachmann, O. The effect of prior hydrothermal alteration on the melting behaviour during rhyolite formation in Yellowstone, and its importance in the generation of low-δ^{18}O magmas. *Earth Planet. Sci. Lett*. **481**, 338–349 (2018).
66. Cook, G. W., Wolff, J. A. & Self, S. Estimating the volume of a large pyroclastic body: the Otowi Member of the Bandelier Tuff, Valles caldera, New Mexico. *Bull. Volcanol.* **78**, 10 (2016).
67. Wilson, C. J. N., Gravley, D. M., Leonard, G. S. & Rowland, J. V.. Volcanism in the central Taupo Volcanic Zone, New Zealand: tempo, styles and controls. *Spec. Publ. IAVCEI* **2**, 225–247 (2009).
68. Downs, D. T. *et al.* (2014). Age and eruptive center of the Paeroa Subgroup ignimbrites (Whakamaru Group) within the Taupo Volcanic Zone of New Zealand. *Geol. Soc. Am. Bull.* **126**, 1131–1144.
69. Forni, F., Degruyter, W., Bachmann, O., De Astis, G. & Mollo, S. Long-term magmatic evolution reveals the beginning of a new caldera cycle at Campi Flegrei. *Sci. Adv.* **4**, (2018).
70. Townsend, M., Degruyter, W., Huber, C. & Bachmann, O. (2019) Magma chamber growth during inter-caldera periods: insights from thermo-mechanical modeling with applications to Laguna del Maule, Campi Flegrei, Santorini, and Aso. *Geochem. Geophys. Geosyst.* **20**, 1574–1591 (2019).
71. Riley, P., Tikoff, B. & Hildreth, W. Transtensional deformation and structural control of contiguous but independent magmatic systems: Mono-Inyo Craters, Mammoth Mountain, and Long Valley caldera, California. *Geosphere* **8**, 740–751 (2012).
72. Allan, A. S. R., Wilson, C. J. N., Millet, M.-A. & Wysoczanski, R. J. The invisible hand: tectonic triggering and modulation of a rhyolitic supereruption. *Geology* **40**, 563–566 (2012).
73. Hildreth, W. & Michael, P. J. Comment and reply on 'Chemical differentiation of the Bishop Tuff and other high-silica magmas through crystallization processes'. *Geology* **11**, 622–624 (1983).
74. Streck, M. L. Evaluation of crystal mush extraction models to explain crystal-poor rhyolites. *J. Volcanol. Geotherm. Res.* **284**, 79–94 (2014).
75. Bachmann, O. & Bergantz, G. W. Gas percolation in upper-crustal silicic mushes as a mechanism for upward heat advection and rejuvenation of near-solidus magma bodies. *J. Volcanol. Geotherm. Res.* **149**, 85–102 (2006).
76. Huber, C., Bachmann, O. & Dufek, J. Thermo-mechanical reactivation of locked crystal mushes: melting-induced internal fracturing and assimilation processes in magmas. *Earth Planet. Sci. Lett.* **304**, 443–454 (2011).
77. Parmigiani, A., Huber, C. & Bachmann, O. Mush microphysics and the reactivation of crystal-rich magma reservoirs. *J. Geophys. Res. Sol. Earth* **119**, 6308-6322 (2014).
78. Wolff, J. A. *et al.* Remelting of cumulates as a process for producing chemical zoning in silicic tuffs: a comparison of cool, wet and hot, dry rhyolitic magma systems. *Lithos* **236–237**, 275–286 (2015).
79. Cashman, K. V. & Giordano, G. Calderas and magma reservoirs. *J. Volcanol. Geotherm. Res.* **288**, 28–45 (2014).
Summarises and synthesises many of the key concept in our views of magmatic systems below caldera volcanoes.

80. Lipman, P. W. Subsidence of ash-flow calderas: relation to caldera size and magma-chamber geometry. *Bull. Volcanol.* **59**, 198–218 (1997).
81. Lipman, P. W. & McIntosh, W. C. Eruptive and noneruptive calderas, northeastern San Juan Mountains, Colorado: where did the ignimbrites come from? *Geol. Soc. Am. Bull.* **120**, 771–795 (2008).
82. Gravley, D. M., Wilson, C. J. N., Leonard, G. S. & Cole, J. W. Double trouble: paired ignimbrite eruptions and collateral subsidence in the Taupo Volcanic Zone, New Zealand. *Geol. Soc. Am. Bull.* **119**, 18–30 (2007).
83. Putirka, K. D. & Tepley III, F.J. (Editors) Minerals, inclusions and volcanic rocks. *Rev. Mineral. Geochem.* **69**, 1–674.
84. Gualda, G. A. R., Ghiorso, M. S., Lemons, R. V. & Carley, T. L. Rhyolite-MELTS: a modified calibration of MELTS optimized for silica-rich, fluid-bearing magmatic systems. *J. Petrol.* **53**, 875–890 (2012).
85. Wilke, S., Holtz, F., Neave, D. A. & Almeev, R. The effect of anorthite content and water on quartz-feldspar cotectic compositions in the rhyolitic system and implications for geobarometry. *J. Petrol*. **58**, 789–819 (2017).
86. Huang, H.-H. *et al.* The Yellowstone magmatic system from the mantle plume to the upper crust. *Science* **348**, 773–776 (2015).
Using tomographic techniques, this paper presented the new discovery at Yellowstone (but now recognised at other centres globally) of the lower-crustal basaltic magma reservoir in addition to the previously known upper-crustal magma reservoir.
87. Jaxybulatov, K. *et al.* A large magmatic sill complex beneath the Toba caldera. *Science* **346**, 617–619 (2014).
88. Quick, J. E., Sinigoi, S., Peressini, G., Demarchi, G., Wooden, J. L. & Sbisa, A. Magmatic plumbing of a large Permian caldera exposed to a depth of 25 km. *Geology* **37**, 603–606 (2009).
89. Otamendi, J. E., Ducea, M. N. & Bergantz, G. W. Geological, petrological and geochemical evidence for progressive construction of an arc crustal section, Sierra de Valle Fertil, Famatinian Arc, Argentina. *J. Petrol*. **53**, 761-800 (2012).
90. Klein, B. Z. & Jagoutz, O. Construction of a trans-crustal magma system: building the Bear Valley Intrusive Suite, southern Sierra Nevada, California. *Earth Planet. Sci. Lett*. **553**, 116624 (2021).
91. Hildreth, W. & Moorbath, S. (1988). Crustal contributions to arc magmatism in the Andes of central Chile. *Contrib. Mineral. Petrol.* **98**, 455-489.
92. Rowe, M. C. *et al.* Development of a continental volcanic field: petrogenesis of pre-caldera intermediate and silicic rocks and origin of the Bandelier magmas, Jemez Mountains (New Mexico, USA). *J. Petrol.* **48**, 2063–2091 (2007).
93. Annen, C. From plutons to magma chambers: thermal constraints on the accumulation of eruptible silicic magma in the upper crust. *Earth Planet. Sci. Lett.* **284**, 409–416 (2009).
94. Wright, H. M. N., Folkes, C. B., Cas, R. A. F. & Cashman, K. V. Heterogeneous pumice populations in the 2.08-Ma Cerro Galan ignimbrite: implications for magma recharge and ascent preceding a large-volume silicic eruption. *Bull. Volcanol*. **73**, 1513–1533 (2011).
95. Cooper, G. F., Wilson, C. J. N., Millet, M.-A. & Baker, J. A. Generation and rejuvenation of a supervolcanic magmatic system: a case study from Mangakino volcanic centre, New Zealand. *J. Petrol.* **57**, 1135-1170 (2016).
96. Barker, S. J., Wilson, C. J. N., Morgan, D. J. & Rowland, J. V. Rapid priming, accumulation and recharge of magma driving recent eruptions at a hyperactive caldera volcano. *Geology* **44**, 323–326 (2016).
97. Goff, F., Warren, R. G., Goff, C. J. & Dunbar, N. Eruption of reverse-zoned upper Tshirege Member, Bandelier Tuff from centralized vents within Valles caldera, New Mexico. *J. Volcanol. Geotherm. Res.* **276**, 82–104 (2014).

98. Matthews, N. E., Huber, C., Pyle, D. M. & Smith, V. C. Timescales of magma recharge and reactivation of large silicic systems from Ti diffusion in quartz. *J. Petrol*. **53**, 1385–1416 (2012).
99. Shamloo, H. I. & Till, C. B. Decadal transition from quiescence to supereruption: petrologic investigation of the Lava Creek Tuff, Yellowstone Caldera, WY. *Contrib. Mineral. Petrol*. **174**, 32 (2019).
100. Wotzlaw, J.-F., Bindeman, I. N., Stern, R. A., D'Abzac, F.-X. & Schaltegger, U. Rapid heterogeneous assembly of multiple magma reservoirs prior to Yellowstone supereruptions. *Sci. Rep.* **5**, 14026 (2015).
101. Chamberlain, K. J., Wilson, C. J. N., Wallace, P. J. & Millet, M.-A. Micro-analytical perspectives on the Bishop Tuff and its magma chamber. *J. Petrol*. **56**, 605–640 (2015).
102. Cooper, K. M. Time scales and temperatures of crystal storage in magma reservoirs: implications for magma reservoir dynamics. *Phil. Trans. R. Soc. Lond*. *A* **377**, 20180009 (2019).
103. Cooper, K. M. & Kent, A. J. R. Rapid remobilization of magmatic crystals kept in cold storage. *Nature* **506**, 480–483 (2014).
104. Barboni, M. *et al.* Warm storage for arc magmas. *Proc. Natl Acad. Sci. USA* **113**, 13959–13964 (2016).
105. Marsh, B. D. On the crystallinity, probability of occurrence, and rheology of lava and magma. *Contrib. Mineral. Petrol.* **78**, 85–98 (1981).
106. Bai, T. *et al*. Teleseismic tomography of the Laguna del Maule volcanic field in Chile. *J. Geophys. Res. Sol. Earth* **125**, e2020JB019449 (2020).
107. Tierney, C. R., Reid, M. R., Vazquez, J. A. & Chesner, C. A. Diverse late-stage crystallization and storage conditions in melt domains from the Youngest Toba Tuff revealed by age and compositional heterogeneity in the last increment of accessory phase growth. *Contrib. Mineral. Petrol*. **174**, 31 (2019).
108. Wolff, J. A., Forni, F., Ellis, B. S. & Szymanowski, D. Europium and barium enrichments in compositionally zoned felsic tuffs: a smoking gun for the origin of chemical and physical gradients by cumulate melting. *Earth Planet. Sci. Lett*. **540**, 116251 (2020).
109. Wallace, P. J., Anderson, A. T. & Davis, A. M. Gradients in H_2O, CO_2, and exsolved gas in a large-volume silicic magma system: interpreting the record preserved in melt inclusions from the Bishop Tuff. *J. Geophys. Res*. **104**, 20097–20122 (1999).
110. Myers, M. L., Wallace, P. J. & Wilson, C. J. N. Inferring magma ascent times and reconstructing conduit processes in rhyolitic explosive eruptions using diffusive losses of hydrogen from melt inclusions. *J. Volcanol. Geotherm. Res*. **369**, 95–112 (2019).
111. Gualda, G. A. R. *et al.* Timescales of quartz crystallization and the longevity of the Bishop giant magma body. *PLoS ONE* **7**, e37492 (2012b).
112. Roberge, J., Wallace, P. J. & Kent, A. J. R. Magmatic processes in the Bishop Tuff rhyolitic magma based on trace elements in melt inclusions and pumice matrix glass. *Contrib. Mineral. Petrol*. **165**, 237–257 (2013).
113. Flaherty, T., Druitt, T. H., Tuffen, H., Higgins, M. D., Costa, F., & Cadoux, A. Multiple timescale constraints for high-flux magma chamber assembly prior to the Late Bronze Age eruption of Santorini (Greece). *Contrib. Mineral. Petrol.* **173**, 75 (2018).
114. Tramontano, S., Gualda, G. A. R. & Ghiorso, M. S. Internal triggering of volcanic eruptions: tracking overpressure regimes for giant magma bodies. Earth and Planetary Science Letters 472, 142–151 (2017).
115. Kennedy, B. M. *et al.* Magma plumbing beneath collapse caldera volcanic systems. *Earth-Sci. Rev.* **177**, 404–424 (2018).
116. Sparks, R. S. J. *et al.* Formation and dynamics of magma reservoirs. *Phil. Trans. R. Soc. Lond*. A **377**, 2018.0019 (2019).
117. Black, B. A. & Andrews, B. J. Petrologic imaging of the architecture of magma reservoirs feeding caldera-forming eruptions. *Earth Planet. Sci. Lett*. **552**, 116572 (2020).

118. Jolles, J. S. R. & Lange, R. A. High-resolution Fe–Ti oxide thermometry applied to single-clast pumices from the Bishop Tuff: a re-examination of compositional variations in phenocryst phases with temperature. *Contrib. Mineral. Petrol.* **174**, 70 (2019).
119. Vazquez, J. A. & Reid, M. R. Probing the accumulation history of the voluminous Toba magma. *Science* **305**, 991–994 (2004).
120. Matthews, N. E. *et al.* Quartz zoning and the pre-eruptive evolution of the ~340-ka Whakamaru magma systems, New Zealand. *Contrib. Mineral. Petrol*. **163**, 87–107 (2012).
121. Chamberlain, K. J., Wilson, C. J. N., Wooden, J. L., Charlier, B. L. A. & Ireland, T. R. New perspectives on the Bishop Tuff from zircon textures, ages and trace elements. *J. Petrol*. **55**, 395–426 (2014).
122. Engi, M. Petrochronology based on REE-minerals: monazite, allanite, xenotime, apatite. *Rev. Mineral. Geochem.* **83**, 365–418 (2017).
123. Kohn, M. J. Titanite petrochronology. *Rev. Mineral. Geochem.* **83**, 419–441 (2017).
124. Schaltegger, U., Schmitt, A. K. & Horstwood, M. S. A. U–Th–Pb zircon geochronology by ID-TIMS, SIMS, and laser ablation ICP-MS: recipes, interpretations, and opportunities. *Chem. Geol.* **402**, 89–110 (2015).
125. Miller, J. S., Matzel, J. E. P., Miller, C. F., Burgess, S. D. & Miller, R. B. Zircon growth and recycling during the assembly of large, composite arc plutons. *J. Volcanol. Geotherm. Res.* **167**, 282–299 (2007).
126. Frazer, R. E., Coleman, D. S. & Mills, R. D. Zircon U-Pb geochronology of the Mount Givens Granodiorite: Implications for the genesis of large volumes of eruptible magma. *J. Geophys. Res. Sol. Earth* **119**, 2907–2924 (2014).
127. Cooper, G. F., Wilson, C. J. N., Charlier, B. L. A., Wooden, J. L. & Ireland, T. R. Temporal evolution and compositional signatures of two supervolcanic systems recorded in zircons from Mangakino volcanic centre, New Zealand. *Contrib. Mineral. Petrol*. **167**, 1018 (2014).
128. Rivera, T. A., Schmitz, M. D., Crowley, J. L. & Storey, M. Rapid magma evolution constrained by zircon petrochronology and ^{40}Ar/^{39}Ar sanidine ages for the Huckleberry Ridge Tuff, Yellowstone, USA. *Geology* **42**, 643–646 (2014).
129. Charlier, B. L. A. *et al.* Magma generation at a large, hyperactive silicic volcano (Taupo, New Zealand) revealed by U-Th and U-Pb systematics in zircons. *J. Petrol.* **46**, 3–32 (2005).
130. Folkes, C. B., de Silva, S. L., Schmitt, A. K. & Cas, R. A. F. A reconnaissance of U-Pb zircon ages in the Cerro Galán system, NW Argentina: prolonged magma residence, crystal recycling, and crustal assimilation. *J. Volcanol. Geotherm. Res.* **206**, 136–147 (2011).
131. Reid, M. R. & Vazquez, J. A. Fitful and protracted magma assembly leading to a giant eruption, Youngest Toba Tuff, Indonesia. *Geochem. Geophys. Geosyst*. **18**, 156–177 (2017).
132. Reid, M. R. How long does it take to supersize an eruption? *Elements* **4**, 23–28 (2008).
133. Chamberlain, K. J., Morgan, D. J. & Wilson, C. J. N. Timescales of mixing and mobilisation in the Bishop Tuff magma body: perspectives from diffusion chronometry. *Contrib. Mineral. Petrol*. **168**, 1034 (2014).
134. Costa, F., Shea, T. & Ubide, T. Diffusion chronometry and the timescales of magmatic processes. *Nat. Rev. Earth Environ.* **1**, 201–214 (2020).
135. Druitt, T. H., Costa, F., Deloule, E., Dungan, M. A. & Scaillet, B. Decadal to monthly timescales of magma transfer and reservoir growth at a caldera volcano. *Nature* **482**, 77–80 (2012).
136. Hughes, G. R. & Mahood, G. A. Silicic calderas in arc settings: characteristics, distribution, and tectonic controls. *Geol. Soc. Am. Bull.* **123**, 1577–1595 (2011).
137. Caricchi, L., Annen, C., Blundy, J., Simpson, G. & Pinel, V. Frequency and magnitude of volcanic eruptions controlled by magma injection and buoyancy. *Nature Geosci.* **7**, 126–130 (2014).
138. Koulakov, I. *et al.* The feeder system of the Toba supervolcano from the slab to the shallow reservoir. *Nat. Comm*. **7**, 12228 (2016).

139. Rowland, J. V., Wilson, C. J. N. & Gravley, D. M. Spatial and temporal variations in magma-assisted rifting, Taupo Volcanic Zone, New Zealand. *J. Volcanol. Geotherm. Res.* **190**, 89–108 (2010).
140. Heath, B. A. *et al.* Tectonism and its relation to magmatism around Santorini volcano from upper crustal *P* wave velocity. *J. Geophys. Res. Sol. Earth* **124**, 10610–10629 (2019).
141. Peterson, D. E. *et al.* Active normal faulting, diking, and doming above the rapidly inflating Laguna del Maule volcanic field, Chile, imaged With CHIRP, magnetic, and focal mechanism data. *J. Geophys. Res. Sol. Earth* **125**, e2019JB019329 (2020).
142. Rowland, J. V. & Sibson, R. H. Extensional fault kinematics within the Taupo Volcanic Zone, New Zealand: soft-linked segmentation of a continental rift system. *N.Z. J. Geol. Geophys.* **44**, 271–283 (2001).
143. Lowenstern, J. B., Smith, R. B. & Hill, D. P. Monitoring super-volcanoes: geophysical and geochemical signals at Yellowstone and other large caldera systems. *Phil. Trans. R. Soc. Lond. A* **364**, 2055–2072 (2006).
144. Singer, B. S. *et al.* Geomorphic expression of rapid Holocene silicic magma reservoir growth beneath Laguna del Maule, Chile. *Sci. Adv*. **4**, eaat1513 (2018).
145. Wilson, C. J. N. Stratigraphy, chronology, styles and dynamics of late Quaternary eruptions from Taupo volcano, New Zealand. *Phil. Trans. R. Soc. Lond. A* **343**, 205-306 (1993).
146. Lehman, J. A., Smith, R. B. & Schilly, M. M. Upper crustal structure of the Yellowstone caldera from seismic delay time analyses and gravity correlations. *J. Geophys. Res.* **87**, 2713–2730 (1982).
147. Miller, D. S. & Smith, R. B. *P* and *S* velocity structure of the Yellowstone volcanic field from local earthquake and controlled source tomography. *J. Geophys. Res.* **104**, 15105–15121 (1999).
148. Husen, S., Smith, R. B., & Waite, G. P. Evidence for gas and magmatic sources beneath the Yellowstone volcanic field from seismic tomographic imaging. *J. Volcanol. Geotherm. Res.* **131**, 397–410 (2004).
149. Farrell, J., Smith, R. B., Husen, S. & Diehl, T. Tomography from 26 years of seismicity revealing that the spatial extent of the Yellowstone crustal magma reservoir extends well beyond the Yellowstone caldera. *Geophys. Res. Lett.* **41**, 3068–3073 (2014).
150. Seats, K. J & Lawrence, J. F. The seismic structure beneath the Yellowstone Volcano Field from ambient seismic noise. *Geophys. Res. Lett.* **41**, 8277–8282 (2014).
151. Jiang, C., Schmandt, B., Farrell, J., Lin, F.-C., Ward, K.M., 2018. Seismically anisotropic magma reservoirs underlying silicic calderas. *Geology* **46**, 727–730.
152. Hata, M. *et al.* Three-dimensional electrical resistivity modeling to elucidate the crustal magma supply system beneath Aso caldera, Japan. *J. Geophys. Res. Sol. Earth* **123**, 6334–6346 (2018).
153. Heise, W., Caldwell, T. G., Bibby, H. M. & Bennie, S. L. Three-dimensional electrical resistivity image of magma beneath an active continental rift, Taupo Volcanic Zone, New Zealand. *Geophys. Res. Lett.* **37**, L10301 (2010).
154. Hildreth, W. Fluid-driven uplift at Long Valley, California: geologic perspectives. *J. Volcanol. Geotherm. Res.* **341**, 269-286 (2017).
155. Flinders, A. F. *et al.* Seismic evidence for significant melt beneath the Long Valley Caldera, California, USA. *Geology* **46**, 799–802 (2018).
156. Hill, D. P., Montgomery-Brown, E. K., Shelly, D. R., Flinders, A. F. & Prejean, S. Post-1978 tumescence at Long Valley caldera, California: a geophysical perspective. *J. Volcanol. Geotherm. Res.* **400**, 106900 (2020).
157. Prudencio, J. & Manga, M. 3-D seismic attenuation structure of Long Valley caldera: looking for melt bodies in the shallow crust. *Geophys. J. Intl.* **220**, 1677–1686 (2020).
158. Hammond, J. O. S. & Kendall, J.-M. Constraints on melt distribution from seismology: a case study in Ethiopia. *Geol. Soc. Lond. Spec. Publ*. **420**, 127–147 (2016).

159. Rasht-Behesht, M., Huber, C. & Mancinelli, N. J. Detectability of melt-rich lenses in magmatic reservoirs from teleseismic waveform modeling. *J. Geophys. Res. Sol. Earth* **125**, e2020JB020264 (2020).
160. Lowenstern, J., Sisson, T., Hurwitz, S. Probing magma reservoirs to improve volcano forecasts. *Eos* **98**, https://doi.org/10.1029/2017EO085189 (2017).
161. Acocella, V., Di Lorenzo, R., Newhall, C. & Scandone, R. An overview of recent (1988 to 2014) caldera unrest: Knowledge and perspectives. *Rev. Geophys*. **53**, 896–955 (2015). **This paper provides an extensive review of global caldera unrest, both eruptive and non-eruptive, highlighting the diversity and complexity in the causes and signals of unrest.**
162. Yellowstone Volcano Observatory. Volcano and earthquake monitoring plan for the Yellowstone Volcano Observatory, 2006-2015. *U.S. Geol. Surv. Sci. Inv. Rep.* **2006-5276**, 1–13 (2006).
163. Waite, G. P. & Smith, R. B. Seismic evidence for fluid migration accompanying subsidence of the Yellowstone caldera. *J. Geophys. Res.* **107**, 2177 (2002).
164. Farrell, J., Smith, R. B., Taira, T., Chang, W. L. & Puskas, C. M. Dynamics and rapid migration of the energetic 2008-2009 Yellowstone Lake earthquake swarm. *Geophys. Res. Lett.* **37**, L19305 (2010).
165. Massin, F., Farrell, J. & Smith, R. B. Repeating earthquakes in the Yellowstone volcanic field: Implications for rupture dynamics, ground deformation, and migration in earthquake swarms. *J. Volcanol. Geotherm. Res*. **257**, 159–173 (2013).
166. Pang, G. *et al.* The 2017-2018 Maple Creek earthquake sequence in Yellowstone National Park, USA. *Geophys. Res. Lett.* **46**, 4653–4663 (2019).
167. Wicks, C., Thatcher, W., Dzurisin, D. & Svarc, J. Uplift, thermal unrest and magma intrusion at Yellowstone caldera. *Nature* **440**, 72–75 (2006).
168. Wicks, C., Dzurisin, D., Lowenstern, J. B. & Svarc, J. Magma intrusion and volatile ascent beneath Norris Geyser Basin, Yellowstone National Park. *J. Geophys. Res. Sol. Earth* **125**, e2019JB018208 (2020).
169. Chang, W.-L., Smith, R. B., Farrell, J. & Puskas, C. M. An extraordinary episode of Yellowstone caldera uplift, 2004-2010, from GPS and InSAR observations. *Geophys. Res. Lett*. **37**, L23302 (2010).
170. Langbein, J. O. Deformation of the Long Valley Caldera, California: inferences from measurements from 1988 to 2001. *J. Volcanol. Geotherm. Res.* **127**, 247–267 (2003).
171. Feng, L. & Newman, A. V. Constraints on continued episodic inflation at Long Valley Caldera, based on seismic and geodetic observations. *J. Geophys. Res.* **114**, B06403 (2009).
172. Tizzani, P. *et al.* Uplift and magma intrusion at Long Valley caldera from InSAR and gravity measurements. *Geology* **37**, 63–66 (2009).
173. Johnston, D. *et al.* Social and economic consequences of historic caldera unrest at the Taupo volcano, New Zealand and the management of future episodes of unrest. *Bull. N.Z. Soc. Earthq. Eng*. **35**, 215–230 (2002).
174. Otway, P. M., Blick, G. H. & Scott, B.J. Vertical deformation at Lake Taupo, New Zealand, from lake levelling surveys, 1979–99. *N.Z. J. Geol. Geophy.* **45**, 121–132 (2002).
175. Illsley-Kemp, F., Barker, S. J., Smith, B., Wilson, C. J. N.. Implications of a supervolcano's seismicity. *Eos* **101(6)**, 28-32 (2020).
176. Bellucci, F., Woo, J., Kilburn, C. R. J. & Rolandi, G. Ground deformation at Campi Flegrei, Italy: implications for hazard assessment. *Geol. Soc. Lond. Spec. Publ*. **269**, 141–157 (2006).
177. De Natale, G. *et al.* The Campi Flegrei caldera: unrest mechanisms and hazards. *Geol. Soc. Lond. Spec. Publ*. **269**, 25–45 (2006).
178. Kong, Q. *et al.* Machine learning in seismology: turning data into insights. *Seismol. Res. Lett.* **90**, 3–14 (2019).
179. Myers, M. L., Wallace, P. J., Wilson, C. J. N., Watkins, J. L. & Liu, Y. Ascent rates of rhyolitic magma at the onset of three caldera-forming eruptions. *Am. Mineral.* **103**, 952-965 (2018).

180. Freitas, D., Manthilake, G. & Chantel J. Simultaneous measurements of electrical conductivity and seismic wave velocity of partially molten geological materials: effect of evolving melt texture, *Phys. Chem. Mineral*. **46**, 535–551 (2019).
181. Carcione, J. M., Farina, B., Poletto, F., Qadrouh, A. N. & Cheng, W. Seismic attenuation in partially molten rocks. *Phys. Earth Planet. Int.* **309**, 106568 (2020).
182. Barberi, F., Corrado, G., Innocenti, F. & Luongo, G. Phlegraean Fields 1982–1984: brief chronicle of a volcano emergency in a densely populated area. *Bull. Volcanol*. **47**, 175–185 (1984).
183. Maj, M. *et al.* Prevalence of psychiatric disorders among subjects exposed to a natural disaster. *Acta Psychol. Scand*. **79**, 544–549 (1989).
184. Longo, M. L. How memory can reduce the vulnerability to disasters: the bradyseism of Pozzuoli in southern Italy. *AIMS Geosci*. **5**, 631–644 (2019).
185. Atwood, E. *Cultural Super Volcano: a Cultural History of Yellowstone's Hot Spot via Eco-Paranoia.* Thesis, Montana State Univ. (2020).
186. Wilson, C. J. N. Volcanoes: characteristics, tipping points and those pesky unknown unknowns. *Elements* **13**, 41–46 (2017).
187. Chesner, C. A. Petrogenesis of the Toba Tuffs, Sumatra, Indonesia. *J. Petrol*. **39**, 397–438 (1998).
188. Rose, W. I., Grant, N. K. & Easter, J. Geochemistry of the Los Chocoyos ash, Quezaltenango Valley, Guatemala. *Geol. Soc. Am. Spec. Pap.* **180**, 87–99 (1979).
189. Takarada, S. & Hoshizumi, H. Distribution and eruptive volume of Aso-4 pyroclastic density current and tephra fall deposits, Japan: A M8 super-eruption. *Front. Earth Sci*. **8**, 170 (2020).
190. Keller, F., Bachmann, O., Geshi, N. & Miyakawa, A. The role of crystal accumulation and cumulate remobilization in the formation of large zoned ignimbrites: insights from the Aso-4 caldera-forming eruption, Kyushu, Japan. *Front. Earth Sci.* **8**, 614267 (2021).
191. Matthews, N. E., Vazquez, J. A. & Calvert, A. T. Age of the Lava Creek supereruption and magma chamber assembly at Yellowstone based on ^{40}Ar/^{39}Ar and U-Pb dating of sanidine and zircon crystals. *Geochem. Geophys. Geosyst*. **16**, 2508–2528 (2015).
192. Crowley, J. L., Schoene, B. & Bowring, S. A. U-Pb dating of zircon in the Bishop Tuff at the millenial scale. *Geology* **35**, 1123–1126 (2007).
193. Wolff, J. A. & Ramos, F. C. Processes in caldera-forming high-silica rhyolite magma: Rb-Sr and Pb isotope systematics of the Otowi Member of the Bandelier Tuff, Valles Caldera, New Mexico, USA. *J. Petrol.* **55**, 345–375 (2014).
194. Cherniak, D. J. & Watson, E. B. Pb diffusion in zircon. *Chem. Geol.* **172**, 5–24 (2000).
195. Ireland, T. R. & Williams, I. S. Considerations in zircon geochronology by SIMS. *Rev. Mineral. Geochem*. **53**, 215–241 (2003).
196. Schmitt, A. K. & Vazquez, J. A. Secondary ionization mass spectrometry analysis in petrochronology. *Rev. Mineral. Geochem*. **83**, 199–230 (2017).
197. Liu, Y. *et al*. Reappraisement and refinement of zircon U-Pb isotope and trace element analyses by LA-ICP-MS. *Chinese Sci. Bull.* **55**, 1535–1546 (2010).
198. Chang, Z., Vervoort, J. D., McClelland, W. C. & Knaack, C. U-Pb dating of zircon by LA-ICP-MS. *Geochem. Geophys. Geosyst*. **7**, Q05009 (2006).

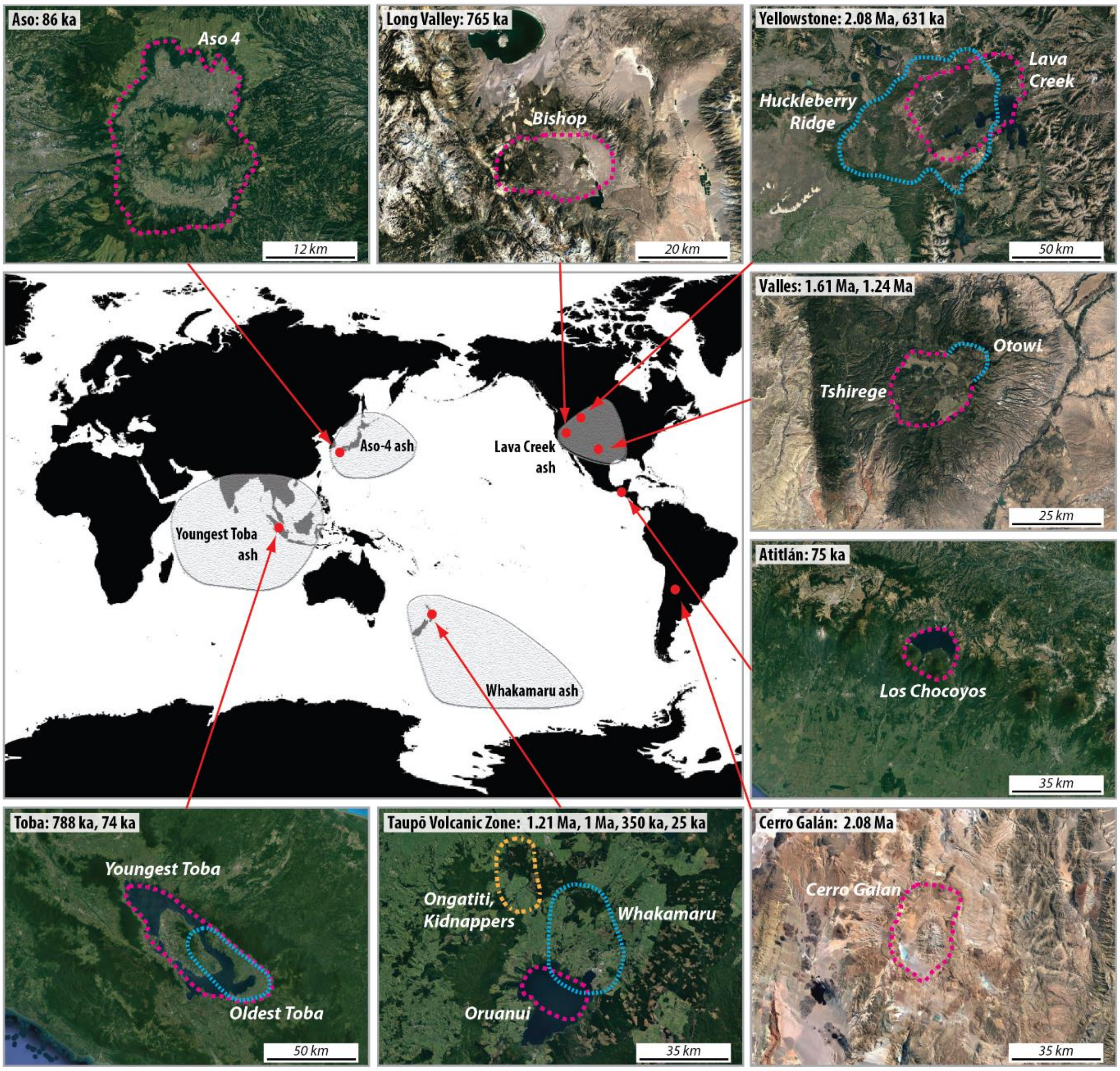

1230
1231
1232 Revised Figure 1

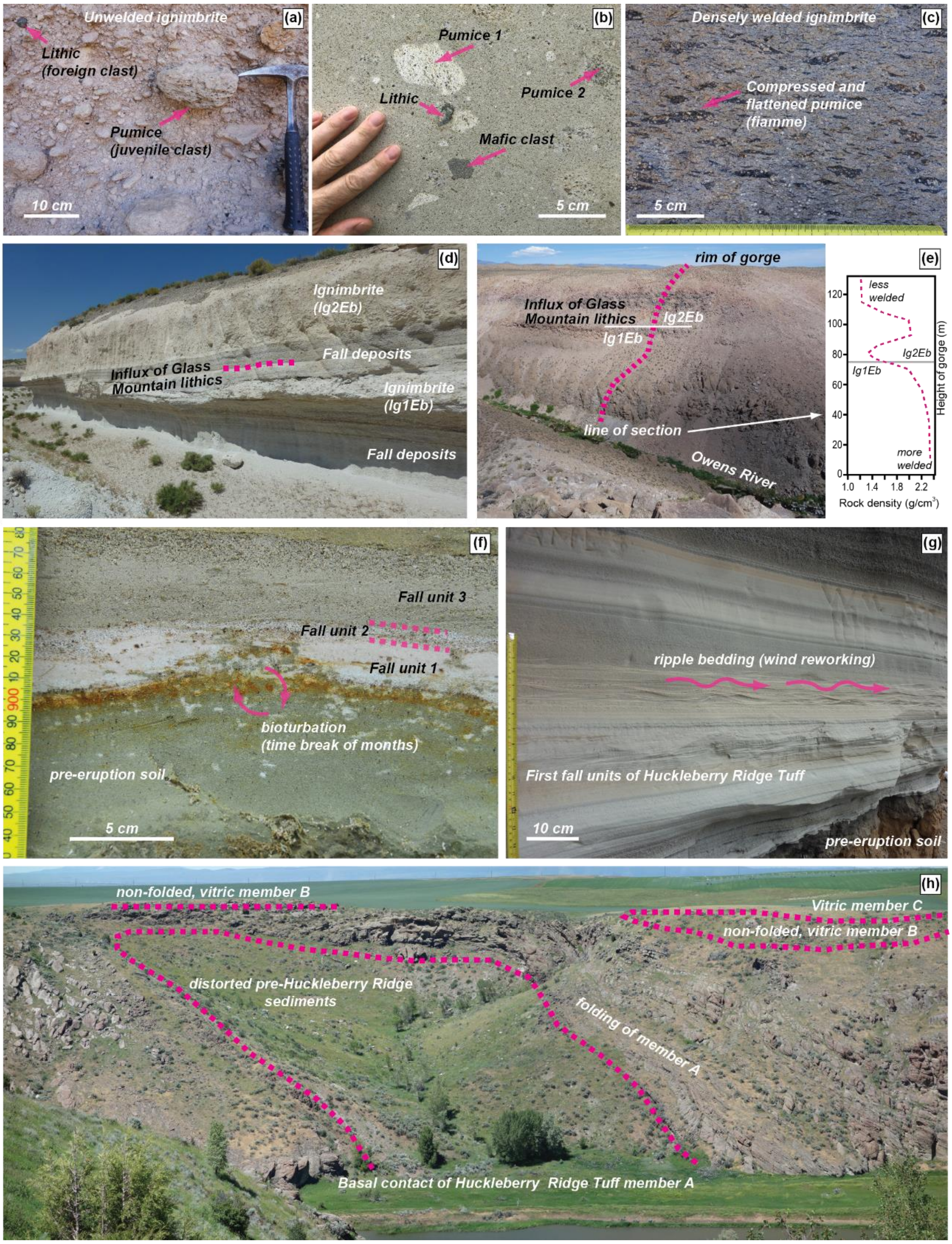

Revised Figure 2

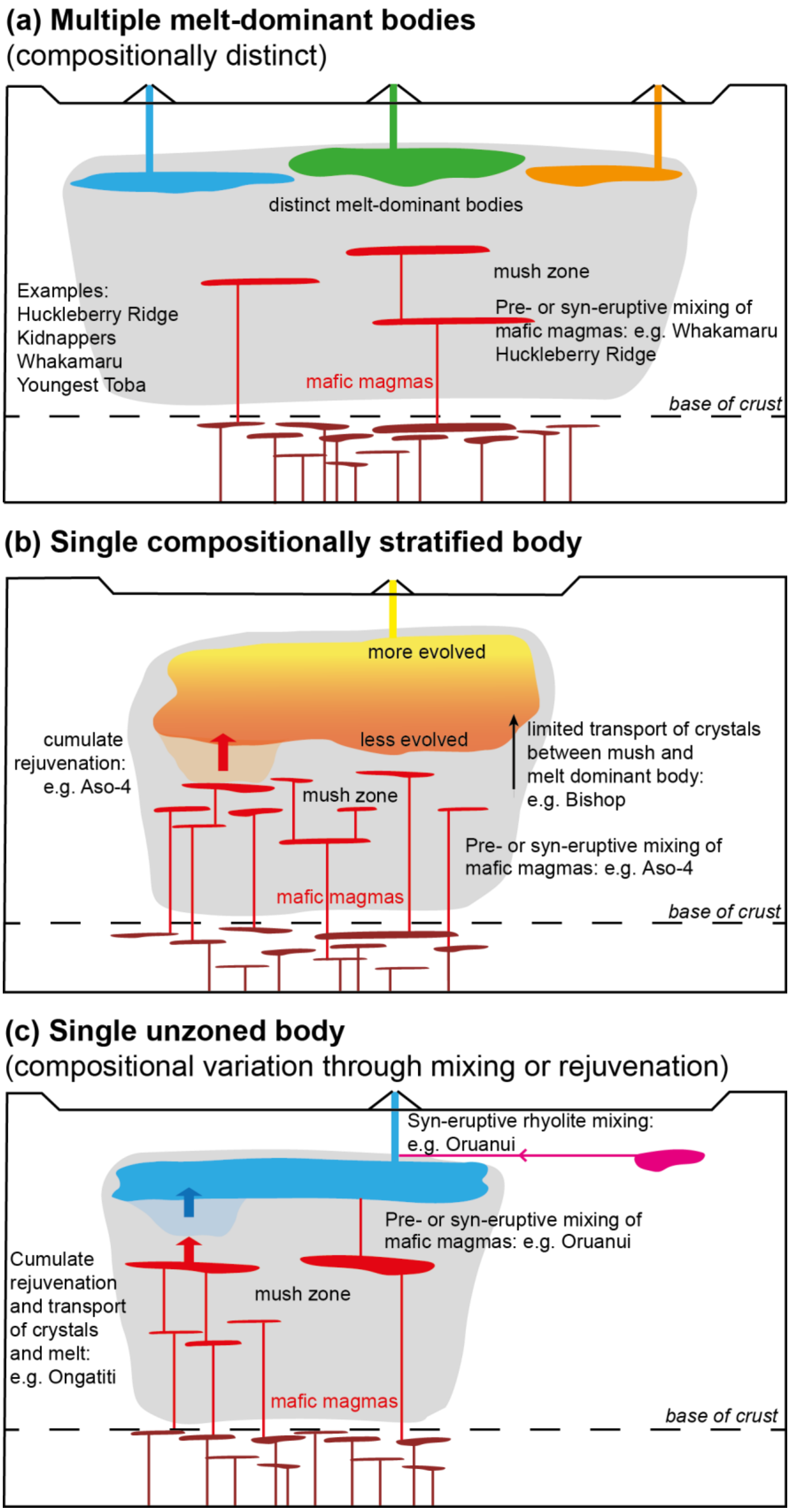

Revised Figure 3

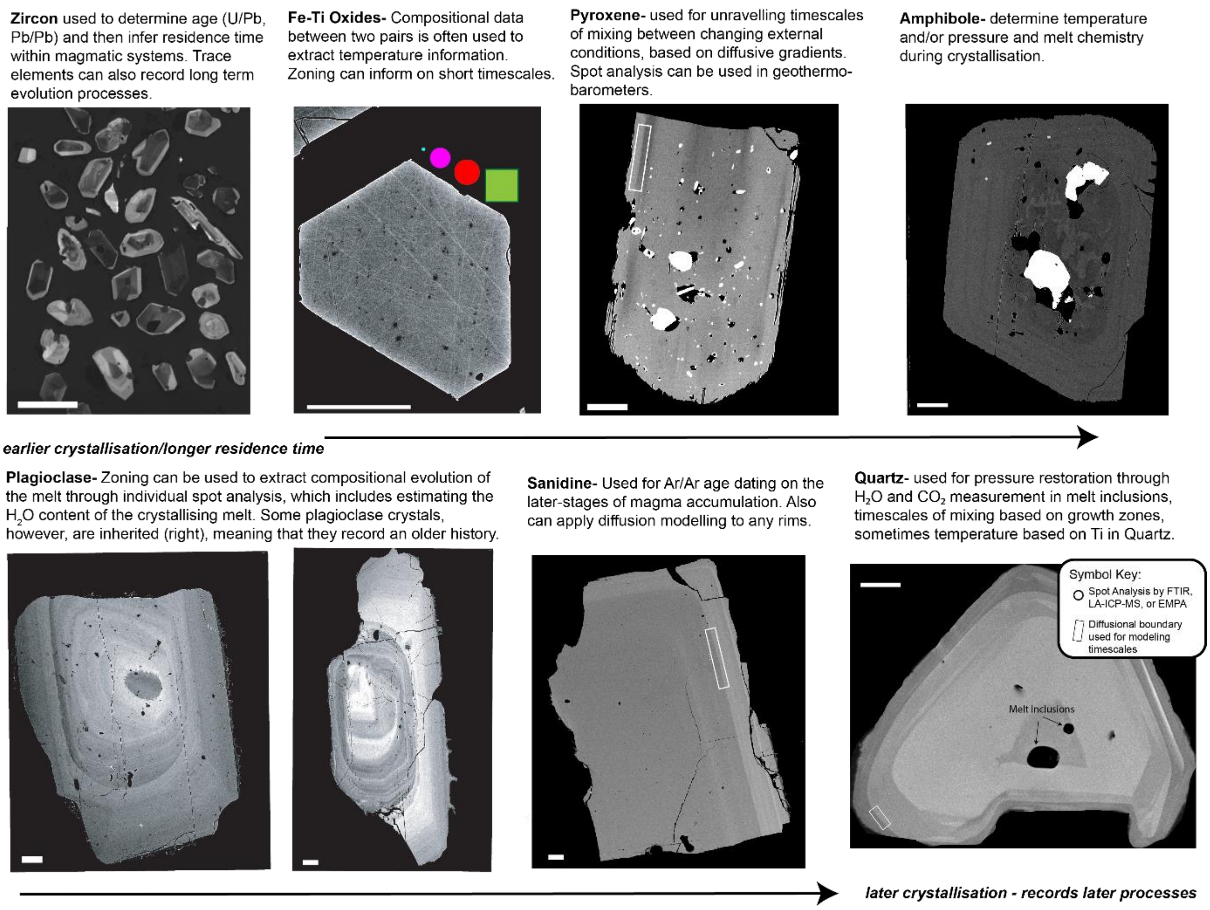

Revised Figure 4

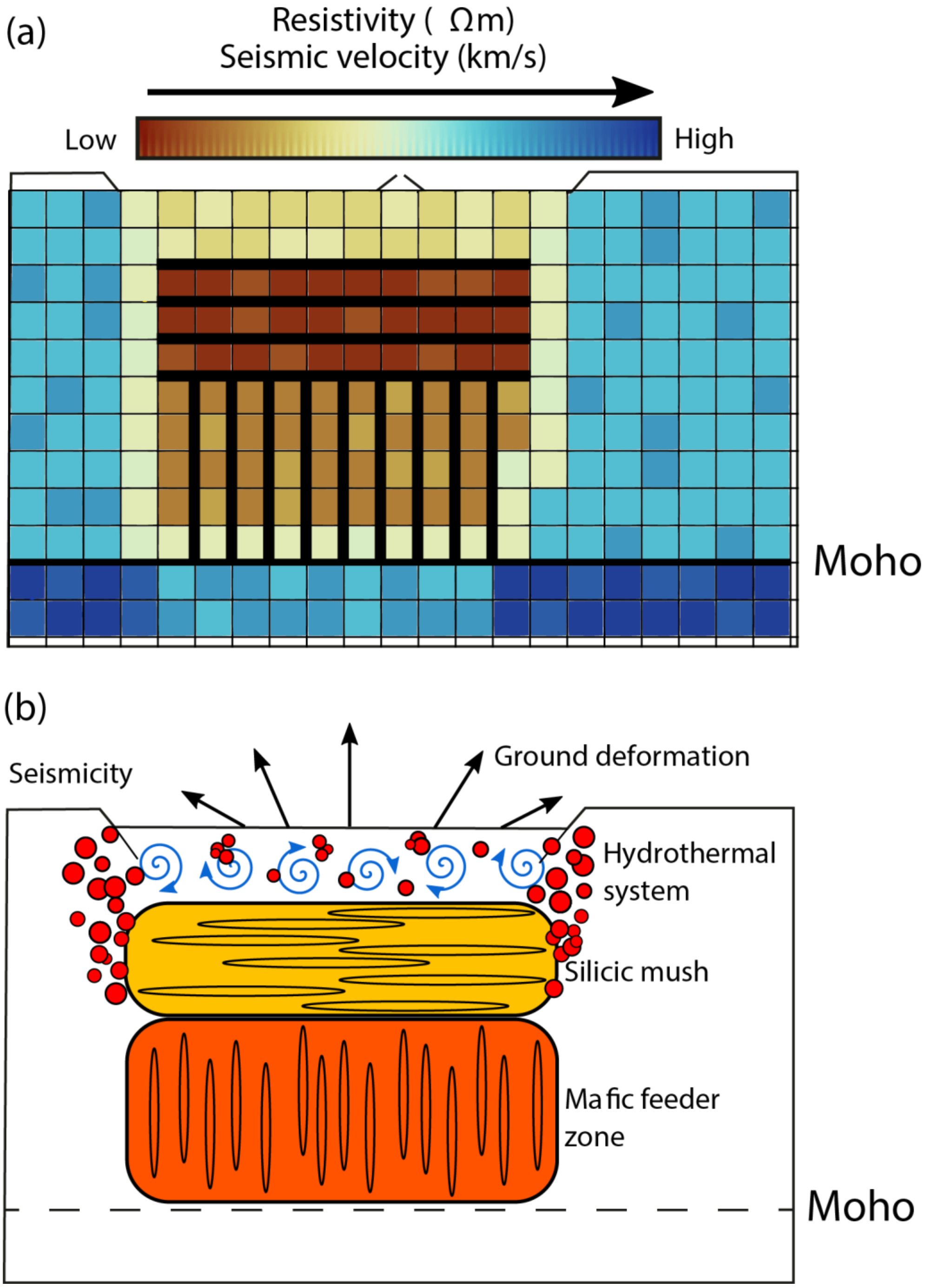

Revised Figure 5

Table 1. Quaternary supereruptive events and their summary features

Eruption, volcano, country	Eruption age (ka)	Approximate volume of magma erupted (km³)	Tectonic setting	Thickness of crust (km)	Number of silicic magmas tapped	Petrological estimates of minimum storage depth (km)	Magma temperature (°C)	Silica range of erupted magmas (wt.%)	State of the magma body at time of eruption	Early fall deposits (with no ignimbrite)?	Time break(s) within the eruption?	References
Oruanui, Taupō, New Zealand	25.4	530	Subduction /rifting	15	Single homogenous with foreign intrusion	4 – 8	760 – 800	73 – 77 *(53 – 63)*	Cooling	Yes	Yes	11, 55, 59, 72, 110, 129, 179
Youngest Toba Tuff, Toba, Indonesia	74	>2800	Subduction/ strike-slip	30 – 40	Multiple, zoned	3 – 6?	700 – 780	69 – 78	Cooling	No	No	21, 36, 40, 41, 44, 107, 119, 131, 187
Los Chocoyos, Atitlán, Guatemala	75	730	Subduction	40 – 50	Single(?) zoned or multiple(?)	Not determined	800 – 950	70 – 78	Not determined	Yes	No	37, 45, 188
Aso-4, Aso, Japan	86	600	Subduction/ rifting	30 – 35	Single, zoned	8 – 15	810 – 910	66 – 71 *(50 – 56)*	Mixing	No	Yes	14, 189, 190
Whakamaru, Whakamaru, New Zealand	350	>1500	Subduction /rifting	15 – 25	Multiple	<6	720 – 820	70 – 77 *(53)*	Warming	No	No	40, 52, 68, 98, 120
Lava Creek, Yellowstone, USA	631	1000	Hotspot	48	Uncertain	3 – 10	820 – 880	74 – 77	Recharging	No?	Yes	22, 35, 60, 99, 100, 191
Bishop, Long Valley, USA	765	>600	Rifting	30 – 40	Single, zoned	4 – 8	700 – 840	73 – 78 *(57 – 72)*	Recharging	Yes	No	10, 34, 49-51, 73, 101, 109-112, 118, 121, 133, 179, 192
Kidnappers, Mangakino, New Zealand	1000	1200	Subduction /rifting	15 – 25	Three	4 – 5.5	770 – 840	71 – 77	Cooling	Yes	No	42,62, 95, 127
Ongatiti, Mangakino, New Zealand	1210	500	Subduction /rifting	15 – 25	Single, homogenous	4 – 6	770 – 840	66 – 73	Warming	No	No	53, 127
Tshirege (Bandelier), Valles, USA	1240	>400	Rifting	<30	Single, zoned	5 – 6	650 – 900	70 – 76	Recharging	Yes	No	13, 56, 92, 97
Otowi (Bandelier), Valles, USA	1610	<550	Rifting	<30	Single, zoned	5 – 6	700 – 880	76 – 78	Recharging	Yes	No	56, 66, 92, 193
Cerro Galan, Cerro Galan, Argentina	2080	630	Subduction	55 – 60	Single?, zoned	4 – 8	790 – 820	68 – 71	Recharging	No	No	54, 94, 130
Huckleberry Ridge, Yellowstone, USA	2080	2500	Hotspot	48	Multiple	4 – 8	800 – 950	66 – 78 *(50 – 66)*	Cooling	Yes	Yes	12, 22, 35, 57, 58, 100, 110, 128, 179

Notes. Not included here is the Oldest Toba Tuff[21], as very little information is known about it. The Tsirege member of the Bandelier Tuff[56] is included as its volume approaches or may exceed the supereruption threshold. The silica range of erupted magmas in roman text indicates those of the main body (or bodies) tapped during the eruption and those italicised in brackets are of minor, less evolved components, where present.